FAM192A/PIP30 regulates Cajal body dynamics by antagonizing PA28γ/coilin interaction

Jonik-Nowak B.[1#], Fesquet D.[1#], Baldin V.[1], Méchali F.[1], Bonne-Andrea C.[1], De Rossi S.[2], Lamond A.I.[3], Boulon S.[1,4*], Coux O.[1*]

[1] Centre de Recherche de Biologie cellulaire de Montpellier (CRBM), UMR5237, CNRS/Université de Montpellier, Montpellier, France

[2] Montpellier Ressources Imagerie facility, Biocampus UMS3426, CNRS, Montpellier, France

[3] Centre for Gene Regulation and Expression, School of Life Sciences, Dundee, UK

[4] Previous address: Centre for Gene Regulation and Expression, School of Life Sciences, Dundee, UK

[#] Contributed equally to this work

* Co-corresponding authors

Running title: PIP30 regulates PA28γ and Cajal body dynamics

Key words: PA28γ; Proteasome; Cajal body; Coilin; SILAC-based proteomics; Casein Kinase 2.

ABSTRACT

PA28γ, a nuclear regulator of the 20S proteasome, is involved in the control of several essential cellular processes, such as cell proliferation and nuclear organization, including Cajal body dynamics. However, the mechanisms controlling PA28γ function in the regulation of nuclear architecture are not known. Here we identify through a SILAC-based proteomics approach a specific and prominent interaction partner of PA28γ, called FAM192A/PIP30. We show that the PA28γ/PIP30 complex is stabilized by Casein Kinase 2-dependent phosphorylation of the PIP30 C-terminal region. PIP30 depletion reduces the number of Cajal bodies in human cells similar to PA28γ overexpression. Importantly, PIP30 depletion also results in the accumulation of PA28γ in residual Cajal body structures, which correlates with an increased interaction between PA28γ and coilin. Altogether our data identify the first regulator of PA28γ, which plays a critical role in Cajal body dynamics by antagonizing the formation of PA28γ/coilin complexes.

INTRODUCTION

Proteasome Activator 28 subunit γ (PA28γ), also known as 11S regulator complex subunit γ or REGγ, is a nuclear regulator of the proteasome (Mao et al., 2008). It functions as a homoheptamer, which, like the other proteasome regulators, opens the gate of the 20S core proteasome complex upon binding and thereby allows the substrates to enter the catalytic chamber (Kish-Trier and Hill, 2013). In contrast with the well-characterized 19S proteasome regulatory particle, which specifically recognizes polyubiquitylated proteins, unfolds them and targets them for degradation by the 20S core proteasome (Tomko and Hochstrasser, 2013), PA28γ, which does not possess any ATPase activity, is believed to activate the degradation of protein substrates in an ATP- and ubiquitin-independent manner (Chen et al., 2007; Li et al., 2007, 2006). In the past decade, various PA28γ protein substrates have been identified, including several cell cycle inhibitors, such as $p21^{Cip1}$, $p16^{INK4}$ and $p19^{ARF}$ (Chen et al., 2007; Kobayashi et al., 2013; Li et al., 2007), suggesting an important role of PA28γ in the control of cell proliferation. In agreement, PA28γ -/- mice display growth retardation and PA28γ -/- MEF cells slightly accumulate in the G1 phase of the cell cycle (Moriishi et al., 2007; Murata et al., 1999). Furthermore, PA28γ was shown to be critical for tumorigenesis (L. Li et al., 2015) and to have anti-apoptotic roles, especially via inhibiting caspase activity when overexpressed (Moncsek et al., 2015). Consistently, overexpression of PA28γ is observed in many cancers (Chen et al., 2013; He et al., 2012; Li et al., 2012; Okamura et al., 2003; Roessler et al., 2006; Xiong et al., 2014) and correlates with adverse clinical prognosis (Chai et al., 2014; J. Li et al., 2015). Other specific PA28γ substrates include SRC-3/AIB (Li et al., 2006), HCV-core protein (Moriishi et al., 2007, 2003), PTTG1/securin-TRβ (Ying et al., 2006), Smurf1 (Nie et al., 2010), SirT1 and SirT7 (Dong

et al., 2013; Sun et al., 2016), CK1δ (Li et al., 2013) and c-myc (S. Li et al., 2015), which link PA28γ to a broad range of essential cellular pathways. However, so far no common structural features, or post-translational modifications, have been uncovered that would explain how these substrates can be specifically recognized by PA28γ and transferred to the catalytic chamber of the 20S core proteasome.

PA28γ also participates in the regulation of nuclear organization. In particular, PA28γ localizes on chromosomes in telophase and plays an important role in the maintenance of chromosomal stability (Zannini et al., 2008). In addition, we, and others, have shown that PA28γ affects the dynamics of various nuclear bodies, including PML bodies, nuclear speckles, nucleoli and Cajal bodies (CBs). For example, PA28γ depletion alters the organization of nuclear speckles and the recruitment of splicing factors to transcription sites (Baldin et al., 2008), increases the number of PML bodies (Zannini et al., 2009) and stimulates ribosomal DNA transcription in the nucleolus (Sun et al., 2016), whereas PA28γ overexpression leads to the disruption of CBs (Cioce et al., 2006).

Importantly, PA28γ plays a crucial role in the cellular stress response. Its expression level is increased upon hydrogen peroxide treatment, possibly to enhance the degradation of oxidatively damaged proteins (Pickering and Davies, 2012) and its association with the 20S core proteasome is increased upon proteotoxic stress, including oxidative stress (Zhang et al., 2015) and proteasome inhibition (Welk et al., 2016). In addition, PA28γ is recruited to DNA damage sites, where it plays a role in DNA repair (Levy-Barda et al., 2011), and it is required for UV-C-induced dispersion of CBs (Cioce et al., 2006). In agreement, PA28γ depletion leads to an increased cellular sensitivity to genotoxic stress (Levy-Barda et al., 2011; Moncsek et al., 2015). Furthermore, PA28γ depletion sensitizes cells to glucose deprivation/energy starvation,

via SirT7 stabilization, which prevents reduction of ribosomal RNA expression and ATP consumption (Sun et al., 2016). Altogether, these observations strongly support an important role of PA28γ in the regulation of nuclear dynamics in response to different types of stresses. However the mechanisms underlying the specific function of PA28γ in these processes and how it is regulated are currently unknown.

CBs are evolutionary conserved subnuclear compartments that bring together factors involved in the processing and assembly of spliceosomal small nuclear RNPs (snRNPs) and small nucleolar RNPs (snoRNPs), including telomerase, in the processing of histone pre-mRNAs and in the recycling of snRNPs (Cioce and Lamond, 2005; Machyna et al., 2015; Matera and Wang, 2014; Nizami et al., 2010; Trinkle-Mulcahy and Sleeman, 2016). CBs are characterized by the presence of coilin. Of note, the depletion of this protein marker induces the dispersion of CBs and alters snRNP biogenesis and RNA splicing fidelity (Wang et al., 2016). Interestingly, in zebrafish, coilin depletion is lethal and the defect in snRNP biogenesis is mostly accountable for this phenotype (Strzelecka et al., 2010). In addition, it has been shown that incomplete and defective snRNPs bind to coilin and accumulate in CBs (Novotný et al., 2015). Altogether, these observations support the idea that coilin and CBs are crucial players in the quality control mechanisms that proofread the processing and assembly of nuclear small non-coding RNPs (Machyna et al., 2015).

Apart from coilin, many factors, including SMN and WRAP53, accumulate in CBs and are essential for their integrity (Girard et al., 2006; Lemm et al., 2006; Mahmoudi et al., 2010). The molecular crowding of these various components in CBs increases the rate of snRNP assembly by 10 fold (Novotný et al., 2011) and orchestrates genome-wide clustering of snRNA, snoRNA and histone genes, which are physically associated with CBs (Dundr et al., 2007; Nizami et al., 2010; Wang et al., 2016). CB formation follows a

dynamic self-organization process (Kaiser et al., 2008) and depends on the active transcription of snRNA and snoRNA genes. Consistently, CB integrity is very sensitive to the cellular environment. For example, CBs are disrupted upon local dynamic force on the cellular surface, transcription inhibition and DNA-damage treatment (Cioce et al., 2006; Hebert, 2013; Poh et al., 2012). Interestingly, we identified PA28γ as an essential player required for UV-C disruption of CBs, correlating with an increased interaction between PA28γ and coilin (Cioce et al., 2006).

Altogether, these observations strongly support an important role of PA28γ in the regulation of nuclear dynamics, notably in response to different types of stresses, even though its specific function and regulation in these processes are still poorly understood. To identify new interaction partners of PA28γ that may participate in the regulation of nuclear organization, and particularly CB dynamics, we used an approach combining endogenous PA28γ immunoprecipitation and SILAC (Stable Isotope Labeling by Amino-Acids in Cell Culture)-based quantitative proteomics (Boulon et al., 2010). Here we report the identification and characterization of FAM192A/PIP30 (PA28γ Interacting Protein 30kDa), a specific interactor of PA28γ. We show that the Casein Kinase 2 (CK2)-dependent phosphorylation of the evolutionary conserved C-terminal domain of PIP30 is important for the formation and/or the stabilization of the PIP30/PA28γ complex. Importantly, PIP30 depletion leads to a decrease in CB number, the unusual accumulation of PA28γ in residual CBs and an increased interaction between PA28γ and coilin. Altogether, our results suggest that PIP30 regulates the function of PA28γ in CB dynamics by modulating its association with coilin.

RESULTS

Identification of a novel interactor of PA28γ

To discover new interactors of PA28γ, we used a high throughput approach combining endogenous PA28γ immunoprecipitation (IP) and SILAC-based quantitative proteomics that allows for the reliable identification of specific partners above the non-specific background of contaminants (Boulon et al., 2010). This strategy enabled us to compare proteins eluted either in the control or in PA28γ IP (Fig. 1A, left panel). Proteins specifically interacting with the bait, i.e., PA28γ, were expected to show Heavy/Light (H/L) ratios higher than 1. In contrast, proteins non-specifically binding to the beads (experimental contaminants) were expected to show H/L ratios close to 1. Proteins with ratios lower than 1 were mostly environmental contaminants, such as keratins.

In this experiment, 68 human protein groups containing at least two unique peptides were quantified and visualized by plotting $\log_2$(H/L ratio) versus $\log_2$(H intensity) (Fig. 1B). PA28γ itself was found with a H/L SILAC ratio close to 15. Other proteins with high H/L SILAC ratios include splicing, transcription and chromatin-associated factors (Table S1), which is in agreement with the role of PA28γ in chromatin dynamics and nuclear speckle organization (Baldin et al., 2008; Zannini et al., 2008). Surprisingly however, only one of the 20S core proteasomal subunits was found, suggesting either that the interaction between PA28γ and the 20S core proteasome was not stable in our experimental conditions and/or that most PA28γ is not associated with the 20S proteasome in the nucleoplasm, in accordance with previous studies (Gao et al., 2004; Welk et al., 2016). Amongst the most enriched interactors of PA28γ was FAM192A, a poorly annotated protein of unknown cellular function that has not been previously

Figure 1

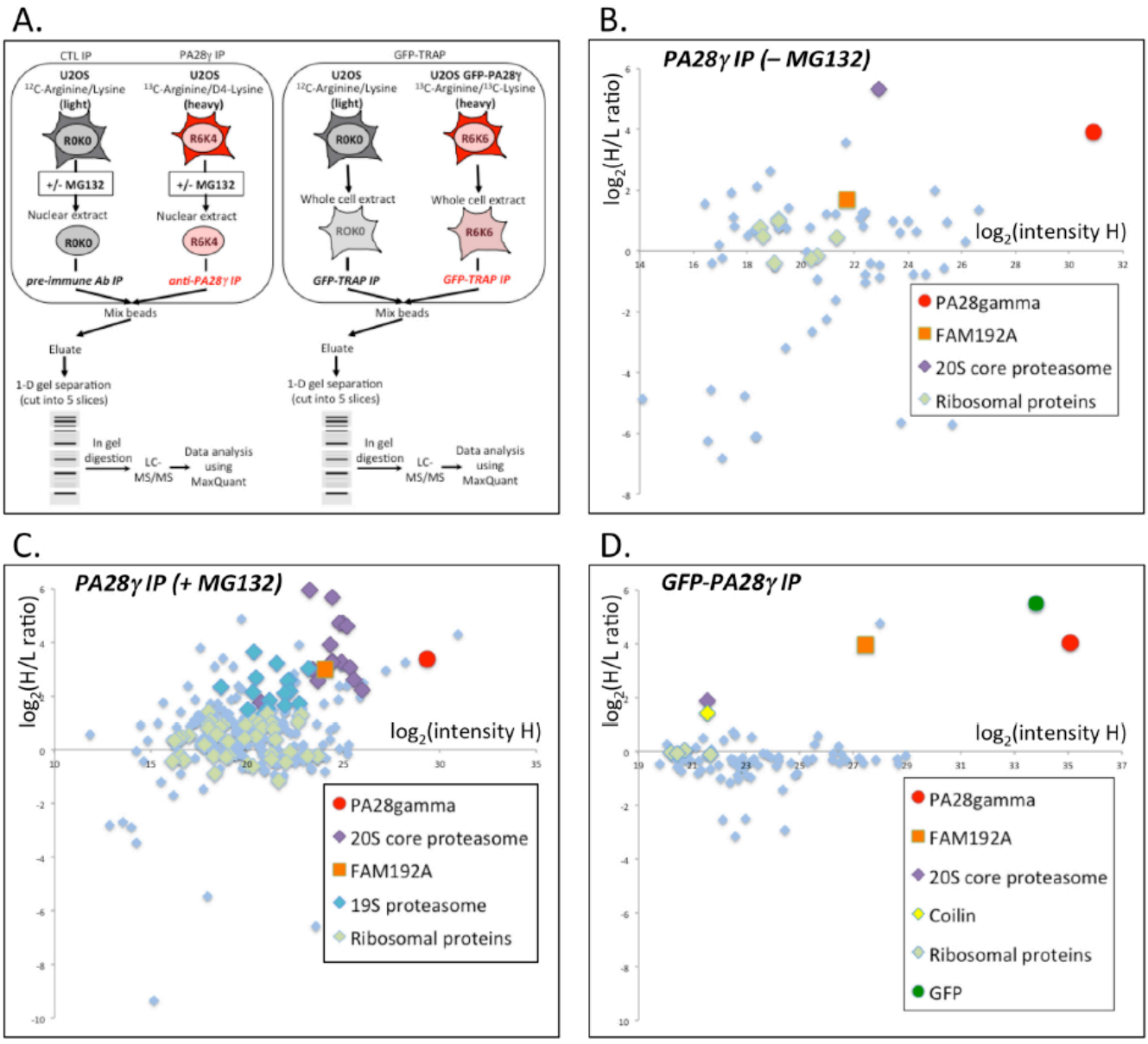

Fig. 1: Identification of a novel interaction partner of PA28γ by a SILAC IP approach

A. ***Design of the SILAC IP experiments.*** For both endogenous PA28γ IPs, control IPs were performed with nuclear extracts prepared from U2OS cells grown in "light", i.e., unlabeled (R_0K_0) medium, while endogenous PA28γ IPs were performed with nuclear extracts prepared from U2OS cells grown in "heavy" (R_6K_4) medium. In addition, in the second experiment, all cells were treated with MG132 (25 μM) for 7 h. For the GFP-PA28γ IP, the control IP was performed with a whole cell extract prepared from U2OS cells grown in "light", i.e., unlabeled (R_0K_0) medium, while the GFP-TRAP IP of GFP-PA28γ was performed with a whole cell extract prepared from U2OS cells grown in "heavy" (R_6K_6) medium. After the immunoprecipitation steps, eluted proteins were *in-gel*

digested with trypsin and peptides analyzed by Liquid Chromatography Tandem Mass Spectrometry (LC-MS/MS) and quantified using MaxQuant.

B. ***Data of the SILAC IP of endogenous PA28γ (untreated cells)*** visualized by plotting $\log_2$(H/L) versus $\log_2$(H intensity) values for all 68 human protein groups quantified by MaxQuant that contained at least two unique peptides identified.

C. ***Data of the SILAC PA28γ IP data (cells treated with MG132)*** visualized by plotting $\log_2$(H/L) versus $\log_2$(H intensity) values for all 267 human protein groups quantified by MaxQuant with a minimum of 2 unique peptides.

D. ***Data of the SILAC GFP-TRAP IP of GFP-PA28γ*** visualized by plotting $\log_2$(H/L) versus $\log_2$(H intensity) values for all 86 protein groups quantified by MaxQuant with a minimum of 2 unique peptides.

In all graphs, the bait (PA28γ) is indicated by a red dot. A novel stable interaction partner of PA28γ, called FAM192A, which is identified in all three IPs with high H/L SILAC ratios, is indicated by an orange square. The different subunits of the 20S core proteasome are indicated by violet diamonds, and the subunits of the 19S regulatory particle by blue diamonds. Ribosomal proteins, which can be considered here as non-specific interaction partners, are indicated by green diamonds.

197 characterized, except for the fact that its expression is induced during skeletal muscle
198 atrophy (Waddell et al., 2016).
199 To identify proteins that may interact with the PA28γ/20S proteasome complexes, we
200 repeated the same experiment in the presence of MG132 (Fig. 1A, left panel and Fig. 1C).
201 In this experiment, 267 human protein groups were quantified (Fig. 1C and Table S2). As
202 anticipated, all 14 α and β subunits of the 20S core proteasome were found with high
203 H/L SILAC ratios this time (violet squares, Fig. 1C), confirming that proteasome
204 inhibition enhances the interaction between the 20S core proteasome and PA28
205 complexes (Shibatani et al., 2006; Welk et al., 2016). It is noteworthy that many subunits
206 of the 19S activator of the proteasome were also identified with high SILAC H/L ratios,
207 suggesting the presence of PA28γ in hybrid proteasomes, with the 20S core binding
208 PA28γ at one end and the 19S regulatory particle at the other end. Interestingly,
209 FAM192A was again identified among the proteins with the highest SILAC ratios in this
210 co-IP experiment, as well as in the GFP-PA28γ SILAC pull-down that we performed in
211 parallel (Fig. 1A, right panel, Fig. 1D and Table S3). Of note, coilin was also identified
212 with a high SILAC ratio in the GFP-PA28γ SILAC pull-down. In conclusion, FAM192A was
213 identified in three distinct experimental settings as a major and specific interaction
214 partner of PA28γ.
215 Although FAM192A is characterized by the presence of an evolutionary conserved N-
216 terminal 100 amino acids domain called NIP30 (NEFA-interacting nuclear protein 30
217 kDa) domain (Fig. 3A), its molecular and cellular functions are unknown. To investigate
218 FAM192A biological roles, we first produced a stable U2OS cell line overexpressing GFP-
219 FAM192A and analyzed GFP-FAM192A interaction partners by a SILAC-based GFP-
220 pulldown approach (Fig. 2A, top panel). The 364 human protein groups quantified in
221 this experiment were visualized by plotting $\log_2$(H/L ratio) versus $\log_2$(intensity H) (Fig.

2A, bottom panel). Interestingly, PA28γ was identified as the most abundant partner of FAM192A. All these observations showing a stable interaction between FAM192A and PA28γ are consistent with a functional link between these two proteins, which was further confirmed in this study. Therefore, since the biological relevance of the name NIP30, which is associated to the FAM192A protein in databases, is unclear, we propose to rename this protein 'PIP30', i.e., PA28γ Interacting Protein of ≈ 30 kDa.

PA28γ and PIP30 interact in the nucleus

To help characterize the function of PIP30, we produced and purified a rabbit polyclonal antibody raised against recombinant full-length PIP30. Western blot analysis of U2OS total cell extracts with this antibody revealed a band migrating at an apparent molecular weight of 35 kDa (Fig. 2B left panel), higher than that predicted by PIP30 cDNA sequence, i.e., 28.9 kDa. However, both this band and the nuclear signal observed by indirect immunofluorescence (Fig.2B, right panel) were lost upon PIP30 depletion by siRNAs (Fig. 2B, left and right panels), demonstrating the specificity of this antibody. In conclusion, endogenous PIP30 is a nucleoplasmic protein, similarly to PA28γ, that migrates at an apparent molecular weight of 35 kDa in western blot analyses.

To investigate the subcellular location of the PA28γ/PIP30 complex, we next performed Proximity Ligation Assays (PLA), using either the combination of PIP30 and PA28γ antibodies or PIP30 antibody alone, as a negative control (Fig. 2C). This approach showed that PIP30 and PA28γ interact in the nucleus, without any evident accumulation of the PIP30/PA28γ complex in specific subnuclear domains (Fig. 2C).

To further characterize the association between PA28γ and PIP30 *in cellulo,* we performed endogenous PIP30 and PA28γ immunoprecipitation assays using whole cell

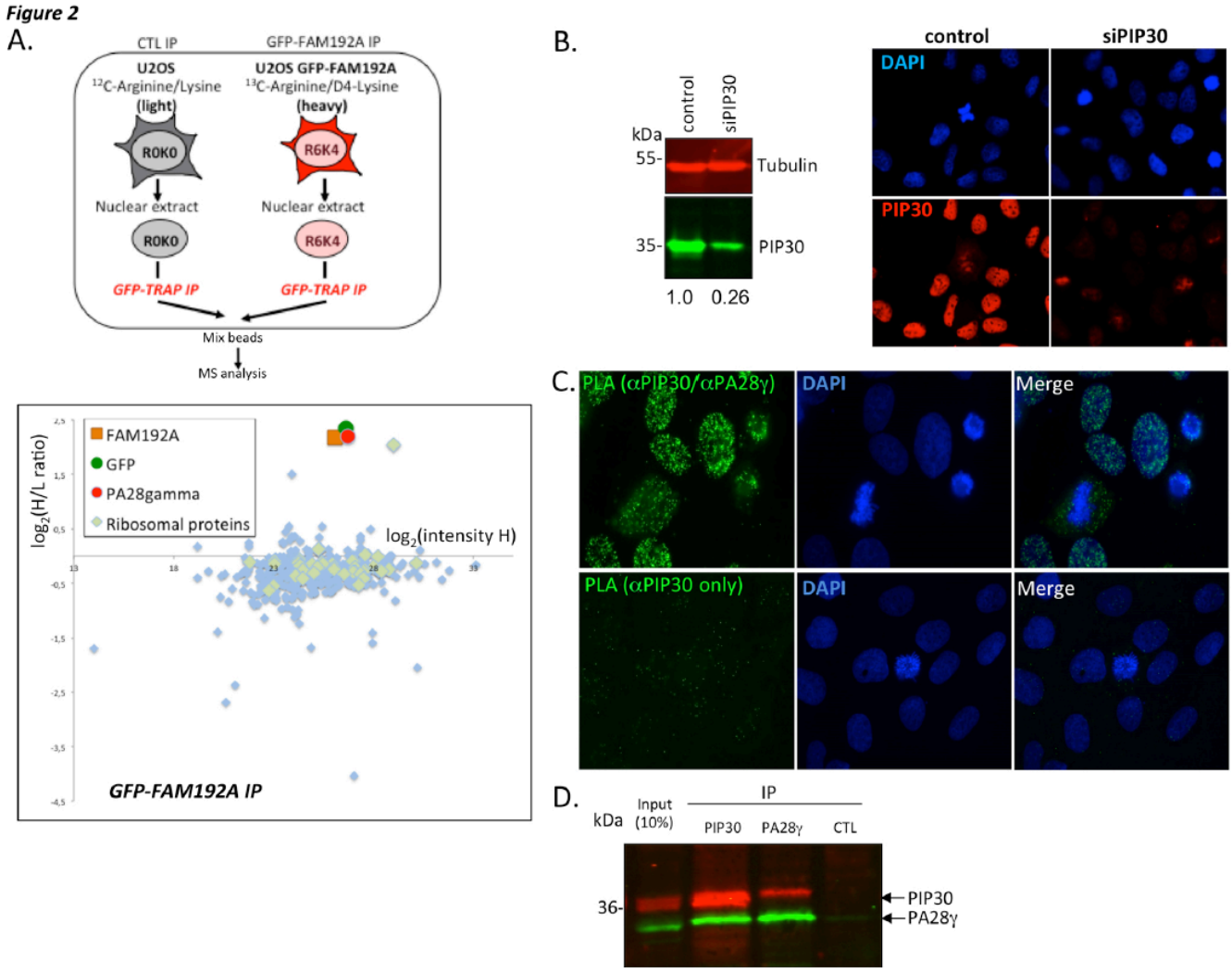

Fig. 2: FAM192A/PIP30 interacts with PA28γ in the cell nucleus

A. ***SILAC GFP-TRAP IP of GFP-FAM192A/PIP30. Top panel: Design of the experiment.*** A double labeling strategy was applied, using U2OS cells stably overexpressing GFP-FAM192A/PIP30. The control IP was performed with a nuclear extract prepared from WT U2OS cells grown in "light", i.e., unlabeled (R_0K_0) medium, while the GFP-FAM192A/PIP30 IP was performed with a nuclear extract prepared from GFP-FAM192A/PIP30 U2OS cells grown in "heavy" (R_6K_4) medium. ***Bottom panel:*** Data of the SILAC GFP-TRAP IP of GFP-FAM192A/PIP30 were visualized by plotting $\log_2$(H/L) versus $\log_2$(intensity H) values for all 364 protein groups quantified by MaxQuant with a minimum of 2 unique peptides. The bait (GFP-FAM192A/PIP30) is indicated by an orange square (peptides for FAM192A/PIP30) and a green dot (peptides for GFP). PA28γ is identified with a high H/L SILAC ratio and indicated by a red dot. As in Fig. 1, ribosomal proteins, which can be considered here as non-specific interaction partners, are indicated by green diamonds.

B. ***Validation of the polyclonal anti-FAM192A/PIP30 antibody***. Cell extracts from U2OS cells treated with either control or FAM192A/PIP30 siRNAs for 48 h were analyzed by western blotting and indirect immunofluorescence, using indicated antibodies.

C. ***FAM192A/PIP30 interacts with PA28γ in the nucleus***. Proximity ligation assay (PLA) was performed on U2OS cells with mouse anti-PA28γ and rabbit affinity purified anti-FAM192A/PIP30 primary antibodies. Green dots reveal places where PA28γ and FAM192A/PIP30 are in close proximity, potentially in a complex (top panel). As a negative control, coverslips with only anti-FAM192A/PIP30 antibody were used (bottom panel).

D. ***A modified form of endogenous FAM192A/PIP30 interacts with endogenous PA28γ in cells***. U2OS cell extracts were subjected to immunoprecipitations with anti-FAM192A/PIP30, anti-PA28γ and control antibodies as described in Materials and Methods, and analyzed by western blotting to detect the presence of endogenous FAM192A/PIP30 (red) and PA28γ (green).

276 extracts prepared from U2OS cells. PIP30 was specifically co-immunoprecipitated with
277 PA28γ. Reciprocally, PA28γ was co-purified with PIP30 (Fig. 2D). Of note, at least 50% of
278 each protein were associated with the other, confirming that PIP30 can be considered as
279 a major interaction partner of PA28γ. In addition, two protein bands were often detected
280 for endogenous PIP30 (Fig. 2D), which may reveal the existence of a post-translationally
281 modified form of the protein. Interestingly, only the slower migrating form of PIP30 was
282 co-purified with PA28γ, suggesting that this modification might be involved in the
283 formation/stabilization of the PIP30/PA28γ complex (Fig. 2D). Altogether, our results
284 reveal that the PIP30/PA28γ complex is located in the nuclear compartment and that the
285 formation of the PIP30/PA28γ complex *in cellulo* may be regulated by post-translational
286 modifications of PIP30.
287
288 *Characterization of PA28γ binding motif in PIP30 sequence*
289 We analyzed the region of PIP30 that is responsible for PA28γ binding by building
290 several PIP30 truncation mutants, which allowed us to demonstrate that the C-terminal
291 domain of PIP30 is critical for PA28γ binding (Fig. 3A). Therefore, we generated a GFP-
292 PIP30 201-254 truncation mutant, thereafter named GFP-PIP30-H201. As shown in Fig.
293 3B, we observed that GFP-PIP30-H201 is able to interact with PA28γ, demonstrating
294 that the last 54 amino acids of PIP30 are necessary and sufficient for PA28γ binding.
295
296 *The C-terminal part of PIP30 is phosphorylated by Casein Kinase 2*
297 Given that a putative post-translational modification of PIP30 might be important for
298 the interaction between PA28γ and PIP30, as mentioned above, we closely examined the
299 C-terminal region of PIP30 and identified a short, serine-rich and acidic sequence

Figure 3

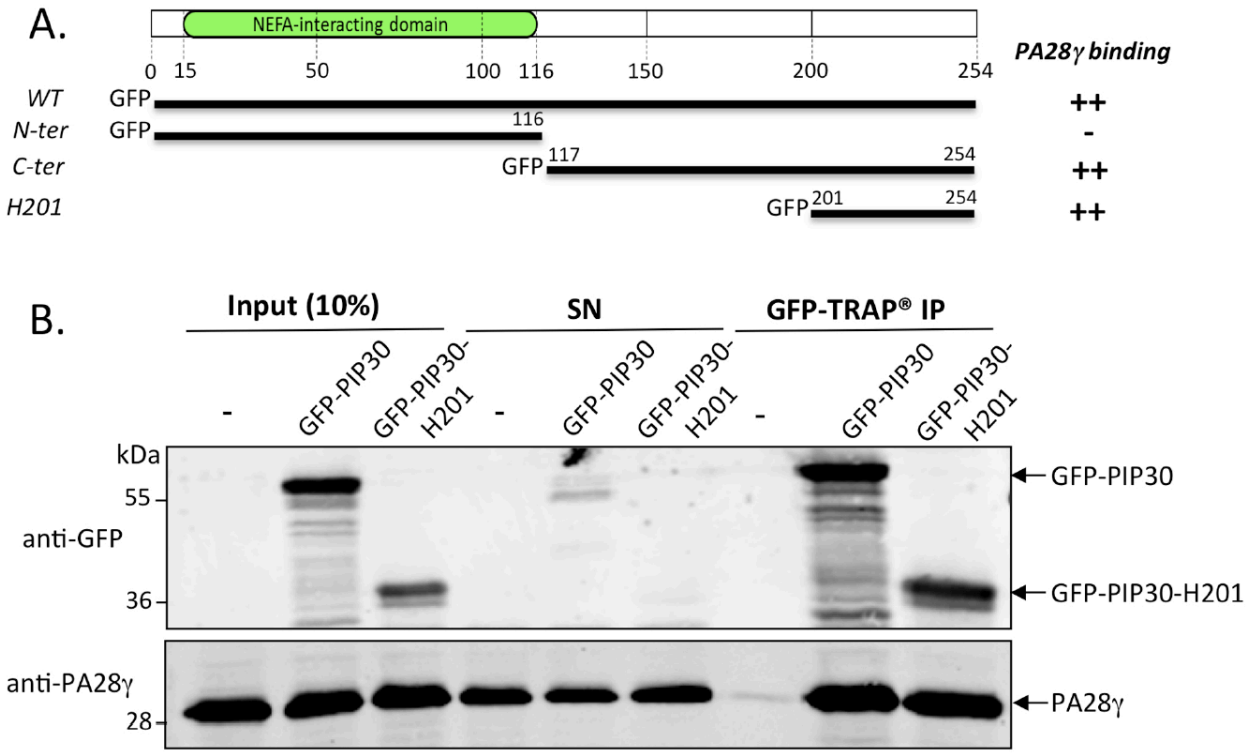

Fig. 3: PA28γ interacts with the C-terminal region of PIP30.

A. ***Analysis of the interaction between several GFP-PIP30 truncation mutants and PA28γ***. GFP pull-down experiments were performed in U2OS cells to immunoprecipitate the overexpressed GFP-PIP30 truncation mutants illustrated in the figure, and the presence of co-eluted endogenous PA28γ was analyzed by western blot. Co-IP results are summarized on the right of the figure.

B. ***The last 54 amino acids of PIP30 are necessary and sufficient for the interaction with PA28γ.*** GFP-PIP30-H201 truncation mutant was transiently overexpressed in U2OS cells and pulled-down using GFP-TRAP®. The presence of co-immunoprecipitated PA28γ was assessed by western blot. Non-transfected cells were used as a negative control and cells transfected with wild type GFP-PIP30 as a positive control. Input represents 10% of the total extract that has been incubated with the beads.

located between amino acids 219 and 232 (SGSSDSESSSDSEG) that is well conserved across evolution, from worm to human (Fig. 4A, black box). This sequence contains a tandem repeat of two SDSE motifs, which correspond to canonical consensus sites for CK2 (consensus site: S/T-X-X-E/D/pS), with putative phosphorylated serine residues being located at positions 222 and 228 (Fig. 4A) (Cesaro and Pinna, 2015; Meggio and Pinna, 2003). Indeed, we could show that GST-PIP30-H201, but not GST, can be phosphorylated by commercial, recombinant CK2 *in vitro* (Fig. 4B), demonstrating that the C-terminal region of PIP30 is a substrate of CK2.

To map the PIP30 residues that are modified by CK2, we inserted several point mutations in GST-PIP30-H201, either by replacing both putative phosphorylated serines, S_{222} and S_{228}, by alanine residues (mutant SS-AA), or by converting the acidic residues within the two CK2 consensus motifs into basic lysine residues (mutants $D_{223}E_{225}$-KK and $D_{229}E_{231}$-KK, respectively) (Fig. 4A). The latter mutations are known to disrupt CK2 substrate recognition (Cesaro and Pinna, 2015). These mutants, together with GST and wild type GST-PIP30-H201, were similarly tested using *in vitro* phosphorylation assays. As anticipated, the mutations of negatively charged residues in $D_{223}E_{225}$-KK and $D_{229}E_{231}$-KK mutants strongly reduced their phosphorylation by CK2, as compared with wild type GST-PIP30-H201, while the GST-PIP30-H201 SS-AA mutant was only partially phosphorylated by CK2 (Fig. 4C). These results confirmed that serine residues 222 and/or 228 can be phosphorylated by CK2 *in vitro* and show that the acidic residues present in this region are critical for CK2 phosphorylation. However, given that the mutation of both S222 and S228 did not completely abolish PIP30-H201 phosphorylation, we hypothesize that other residues within the C-terminal domain may also be phosphorylated by CK2. This is consistent both with the observation that CK2 can phosphorylate residues that are located at positions n-1 and/or n-3 upstream the

Figure 4

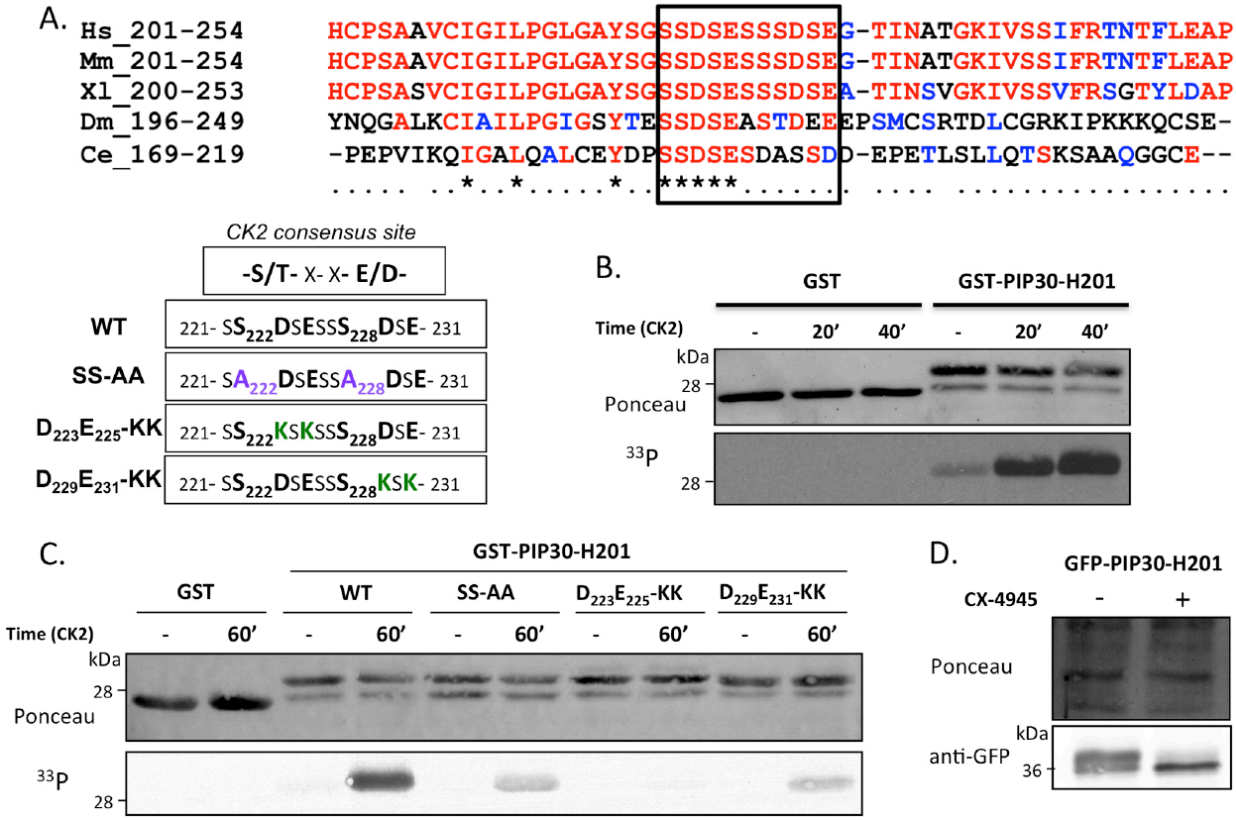

Fig. 4: The C-terminal region of PIP30 is phosphorylated by Casein Kinase 2 *in vitro* and *in cellulo*

A. The 221-SSDSESSSDSE-231 serine-rich region of PIP30 (black box) is conserved from C. elegans to human and contains two typical consensus sites for CK2. Sequences of SS-AA, $D_{223}E_{225}$-KK and $D_{229}E_{231}$-KK PIP30 mutants are indicated, with the mutated residues appearing in violet (SS-AA) and in green ($D_{223}E_{225}$-KK and $D_{229}E_{231}$-KK). UniProtKB accession numbers are as follows : Hs Q9GZU8; Mm : Q91WE2; Xl: Q7ZYN4; Dm: Q7JWU9; Ce: O17594.

B. ***The GST-PIP30-H201 truncation mutant is phosphorylated by CK2 in vitro***

C. ***Point mutations of the acidic residues in the CK2 motifs strongly reduce the phosphorylation of GST-PIP30-H201 in vitro.*** Purified GST, GST-PIP30-H201 and GST-PIP30-H201 mutants were incubated with CK2, in the presence of [^{33}P]-ATP for the indicated times. The presence of GST-tagged proteins was revealed by Ponceau and their phosphorylation was detected by autoradiography.

D. ***The inhibition of CK2 prevents the phosphorylation of GFP-PIP30-H201 in cellulo.*** U2OS cells were transiently transfected with GFP-PIP30-H201 and then either treated, or not, with CX-4945 CK2 inhibitor (10 μM) for 24 h. After SDS-PAGE, GFP-PIP30-H201 was visualized by western blot using an anti-GFP antibody.

358 acidic residues (Meggio and Pinna, 2003), which is the case for S222, S228 and several
359 other serine residues in the serine-rich region of PIP30, and with the well-documented
360 property of CK2 to catalyze the generation of phosphoserine stretches (Cesaro and
361 Pinna, 2015).
362 To verify whether the PIP30 C-terminus is also phosphorylated by CK2 *in cellulo*, cells
363 transiently expressing GFP-PIP30-H201 were either treated, or not, with the selective
364 CK2 inhibitor CX-4945 (Pierre et al., 2011) and GFP-PIP30-H201 was analyzed by
365 western blotting. Interestingly, in the absence of CK2 inhibitor, we observed two bands
366 for GFP-PIP30-H201 (Fig. 4D), as previously shown for endogenous PIP30 (Fig. 2D). In
367 the presence of CK2 inhibitor, the slow-migrating band disappeared while the fast-
368 migrating band became stronger (Fig. 4D), consistent with the upper band
369 corresponding to the phosphorylated form and the lower band corresponding to the
370 non-phosphorylated form of the PIP30-H201 fragment. As shown and discussed below,
371 a similar result is obtained for the endogenous PIP30 protein. Therefore, we conclude
372 that CK2 inhibition reduces the phosphorylation of PIP30-H201, confirming that the C-
373 terminal region of PIP30 is phosphorylated in a CK2-dependent manner in cells.
374
375 *CK2-dependent phosphorylation of PIP30 is important for its interaction with PA28γ*
376 Given that PIP30 is phosphorylated in a region that is critical for PA28γ binding, we next
377 considered whether PIP30 phosphorylation might influence the formation/stabilization
378 of the PIP30/PA28γ complex. To test this hypothesis, recombinant GST and GST-PIP30-
379 H201 were either phosphorylated, or not, by CK2 and then incubated with purified and
380 active recombinant PA28γ. The amount of PA28γ co-isolated with GST-tagged proteins
381 after pull-down was analyzed by western blotting (Fig. 5A, left panel). We observed that

382 PA28γ preferentially interacts with CK2-phosphorylated GST-PIP30-H201 (Fig. 5A, left
383 panel).
384 We then performed the same assay with previously described GST-PIP30-H201 mutants
385 SS-AA, $D_{223}E_{225}$-KK and $D_{229}E_{231}$-KK, which were pre-incubated with CK2, and then
386 PA28γ, before pull-down. Interestingly, the interaction between PA28γ and all three
387 GST-PIP30-H201 mutants was impaired, as compared with wild-type GST-PIP30-H201
388 (Fig. 5A, right panel), showing that CK2 phosphorylation of the PIP30 C-terminus plays
389 an important role in stabilizing the PIP30/PA28γ complex.
390 Next, we analyzed the interaction of PA28γ with the same mutants (in the context of
391 GFP-fused PIP30 full-length protein) in cells. U2OS cells were transfected with either
392 wild type GFP-PIP30, -SS-AA, -$D_{223}E_{225}$-KK and -$D_{229}E_{231}$-KK PIP30 mutants or a
393 truncated mutant, GFP-PIP30 1-199, unable to interact with PA28γ. The co-
394 immunoprecipitation of GFP-tagged proteins and endogenous PA28γ was analyzed by
395 western blotting. As expected, PA28γ was co-immunoprecipitated with wild type GFP-
396 PIP30, but not with the GFP-PIP30 1-199 truncation mutant (Fig. 5B). Interestingly, the
397 amount of PA28γ co-immunoprecipitated with GFP-PIP30 SS-AA was lower than with
398 wild type GFP-PIP30, and almost null with $D_{229}E_{231}$-KK (Fig. 5B) and $D_{223}E_{225}$-KK (Fig.
399 S1) acidic mutants. Thus, mutations altering the CK2 consensus site and therefore
400 inhibiting PIP30 phosphorylation, consistently decrease its ability to form a stable
401 complex with PA28γ in cells. It is noteworthy that the mutation of acidic residues had a
402 stronger impact on PA28γ binding than the mutation of serines 222 and 228 (Fig. 5B),
403 which reflects the absolute requirement of these residues for PIP30 interaction with
404 CK2 and/or PA28γ.
405

Figure 5

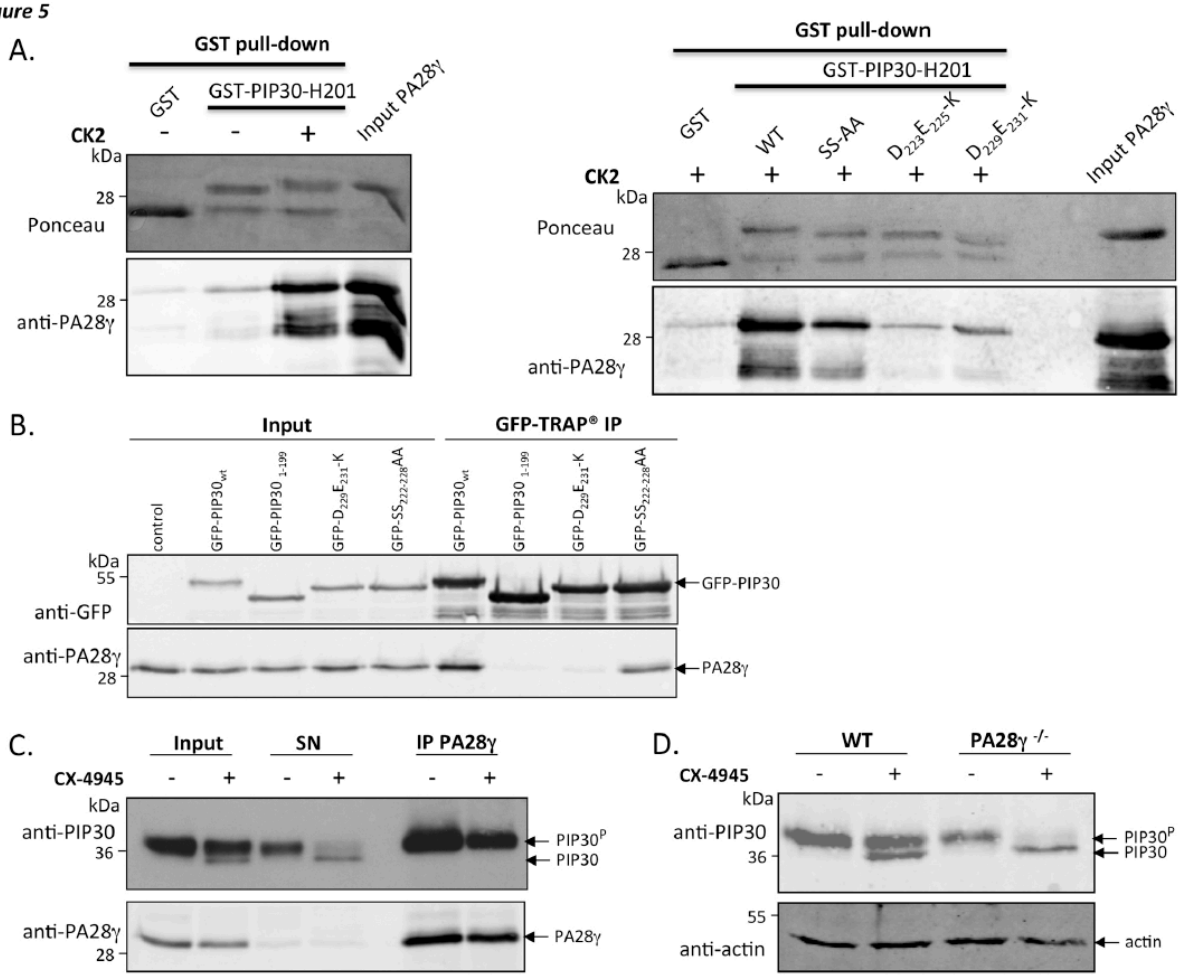

Fig. 5: The CK2-dependent phosphorylation of PIP30 C-terminal region is important for the interaction between PIP30 and PA28γ

A. ***The phosphorylation of GST-PIP30-H201 by CK2 is important for its interaction with PA28γ in vitro.*** **Left panel:** GST and GST-PIP30-H201 were either phosphorylated, or not, by CK2, incubated with recombinant PA28γ and then pulled-down using glutathione sepharose beads. The presence of co-eluted PA28γ was analyzed by western blot using an anti-PA28γ antibody. **Right panel:** Point mutations in the CK2 motif of GST-PIP30-H201 strongly reduce the interaction between GST-PIP30-H201 and PA28γ.

B. Point mutations in the CK2 motif of GFP-PIP30 strongly reduce the interaction between GFP-PIP30 and PA28γ in cellulo. U2OS cells were transiently transfected with wild type and various mutants of PIP30 fused to GFP. GFP-tagged proteins were pulled-down using GFP-TRAP® beads and the presence of co-immunoprecipitated PA28γ was assessed by western blot. Wild type GFP-PIP30 was used as a positive control, GFP-PIP30 1-199 mutant as a negative control.

C. PA28γ interacts with the phosphorylated form of endogenous PIP30 in cellulo. Endogenous PA28γ was immunoprecipitated from U2OS cells either treated, or not, with CX-4945 (10 μM) for 24 h. The presence of co-immunoprecipitated PA28γ was assessed by western blot. The input and unbound (SN) fractions were also analyzed. After CX-4945 treatment, two bands appear for endogenous PIP30, the phosphorylated form ($PIP30^{P}$) and the unphosphorylated form (PIP30), as indicated.

D. The association between PA28γ and PIP30 protects PIP30 from dephosphorylation. Wild type and PA28γ $^{-/-}$ U2OS cells were either treated, or not, with CX-4945 (10 μM) for 24 h and the PIP30 PAGE migration profile was analyzed by western blot. As in Fig. 5C, the phosphorylated form ($PIP30^{P}$) and the unphosphorylated form of PIP30 are indicated.

Finally, we immunoprecipitated PA28γ from U2OS cells, either treated, or not, with CX-4945. In the control cell extract, endogenous PIP30 appeared as only one band, most likely corresponding to the phosphorylated form of PIP30 (Fig. 5C). After CX-4945 treatment, a lower band, corresponding to the dephosphorylated form of PIP30, appeared. Interestingly, only the upper band of PIP30 was retrieved upon PA28γ immunoprecipitation (Fig. 5C), consistent with PA28γ predominantly interacting with the CK2-phosphorylated form of PIP30 and far less with the non-phosphorylated one. Intriguingly, only a minor fraction of endogenous PIP30 was dephosphorylated upon CK2 inhibition (Fig. 5C). We hypothesize that the phosphorylation of endogenous PIP30 might be stabilized by its interaction with PA28γ. To check this, we compared the effect of CK2 inhibition on PIP30 phosphorylation in both wild-type and PA28γ -/- U2OS cells (Fig. S2A, left panel). These cells were either treated, or not, with CX-4945 and the PIP30 migration profile in SDS-PAGE was analyzed by western blotting (Fig. 5D). In PA28γ -/- cells, contrary to U2OS cells, the lower PIP30 band was predominantly present upon CK2 inhibition (Fig. 5D), suggesting that first, PIP30 phosphorylation is PA28γ-independent and second, that the association between PA28γ and PIP30 protects PIP30 from dephosphorylation. This was confirmed by the fact that, in contrast to free PIP30, i.e., not associated to PA28γ, PA28γ-bound PIP30 could not be dephosphorylated by λ-phosphatase (Fig. S2B). Altogether, our results show that PA28γ predominantly binds the phosphorylated form of PIP30, and that once the complex is formed and stabilized, it may sterically hinder phosphatases from accessing PIP30 phosphorylation sites and thus protect PIP30 from dephosphorylation.

PIP30 affects Cajal body dynamics

462 To investigate the biological significance of this newly characterized interaction
463 between PA28γ and PIP30, we checked whether PIP30 depletion could alter the known
464 function of PA28γ in CB dynamics, since we have previously shown that PA28γ
465 overexpression leads to the disruption of CBs in different cell types (Cioce et al., 2006).
466 To compare the effect of PIP30 and PA28γ depletion on CB integrity, we produced U2OS
467 PA28γ -/- and PIP30 -/- cells using the CAS9/CRISPR gene editing technology (Fig. S2A,
468 left and right panels). U2OS PIP30 -/- cells did not show obvious proliferation defects, as
469 assessed by videomicroscopy and flow cytometry analyses, suggesting that PIP30, like
470 PA28γ, is not essential for cell viability in normal growth conditions. The cellular content
471 of CBs was investigated by immunofluorescence combined to an automated image
472 analysis, which measured the number, the mean size and the mean intensity of CBs per
473 cell nucleus, CBs being defined here as endogenous coilin dots whose intensity is
474 superior to a certain threshold (see Material and Methods). The results are presented in
475 Fig. 6.
476 First, we found that the majority of wild-type U2OS cells display CBs (80%), with an
477 average of 2-3 CBs per nucleus, as reviewed in (Morris, 2008). Second, we observed that,
478 unlike PA28γ overexpression, PA28γ depletion had no effect on the percentage of CB
479 positive cells (approximately 80%). However, CBs were more numerous (often more
480 than 3 CBs per nucleus) and slightly smaller in U2OS PA28γ -/- cells as compared with
481 wild-type U2OS (Fig. 6). In contrast, PIP30 depletion induced a significant reduction in
482 the percentage of CB positive cells (down to 40%). In addition, the average number of
483 residual CBs per nucleus in PIP30 -/- cells was strongly decreased (1-2 CBs per nucleus).
484 This shows that CB formation and/or stability is impaired upon PIP30 depletion,
485

Figure 6

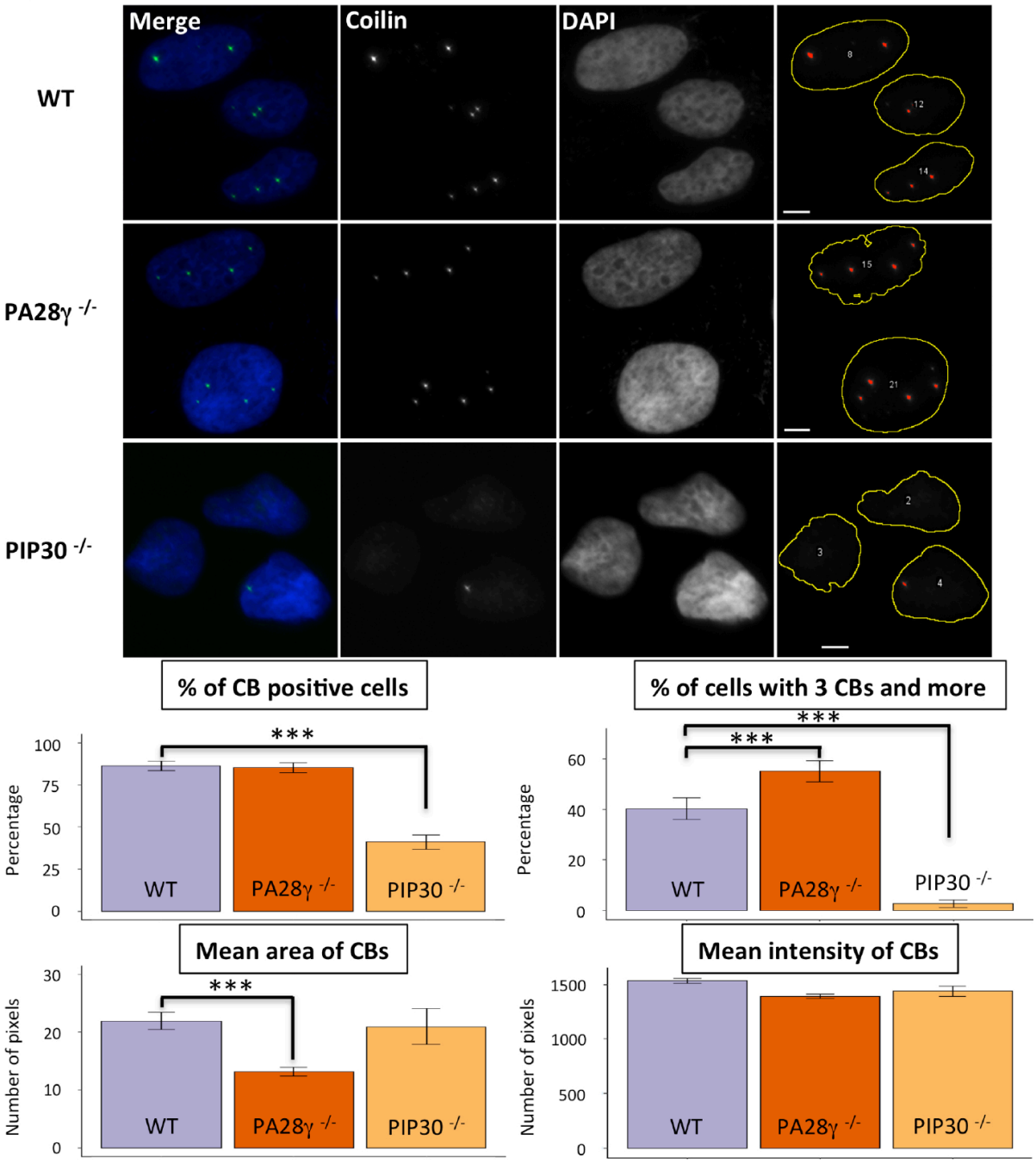

Fig. 6: PA28γ and PIP30 depletions have differential effects on CB dynamics. Wild type, PA28γ $^{-/-}$ and PIP30 $^{-/-}$ U2OS cells were analyzed by immunofluorescence. The DAPI signal was used to delineate the nuclei, each nucleus being considered as a Region of Interest (ROI) (delineated by a yellow line in the right panels). The coilin signal (red dots in the right panels) was used to quantify the number, the mean size and the mean intensity of CBs per nucleus, as summarized in the graphs (see Materials and Methods for details). Data represent the mean of two independent experiments (n= 526 WT, 532 PA28γ $^{-/-}$ and 503 PIP30 $^{-/-}$ cells). Bars, 10 µm. Asterisks *** indicate p-values < 0,001.

whereas PA28γ depletion has an opposite effect, suggesting that PIP30 could modulate the function of PA28γ in the regulation of CB dynamics.

PIP30 depletion induces the accumulation of PA28γ in Cajal bodies

Interestingly, we observed that PIP30 depletion, whether accomplished either by RNA interference or by knock-out of the gene, induced, in a fraction of cells, the accumulation of PA28γ in nuclear dots, which were not detectable in control cells (Fig. 7A, green panels). These PA28γ dots could clearly be considered as residual CBs, as they all colocalized with coilin and disappeared upon coilin knockdown (Fig. 7A, red panels). Reciprocally, all residual CBs contained PA28γ. Of note, PA28γ not only colocalized with coilin in those nuclear dots, but also with other proteins known to concentrate in CBs, such as WRAP53 (also named TCAB1 or WDR79) (Fig. S3A). Interestingly, the overexpression of GFP-PIP30 in PIP30-depleted cells abrogated the accumulation of PA28γ in CBs (Fig. S3B), therefore demonstrating that the accumulation of PA28γ in CBs is indeed due to the absence of PIP30 in these cells.

To check whether the 20S core proteasome accumulated in CBs together with PA28γ, we analyzed the localization of endogenous α4 subunit of the 20S core proteasome in PIP30-depleted cells. Although PA28γ accumulated in the residual CBs in these cells, as expected, we could not detect any accumulation of α4 subunit in these structures (Fig. 7B). Interestingly, bortezomib treatment, which is known to inhibit proteasome activity and to increase the association between PA28γ and the 20S core proteasome (Welk et al., 2016), interfered with the accumulation of PA28γ in residual CBs upon PIP30 depletion (Fig. 7C). Altogether, these results indicate that PA28γ is mostly not associated with the 20S core proteasome in the residual CB structures observed in PIP30-depleted

Figure 7

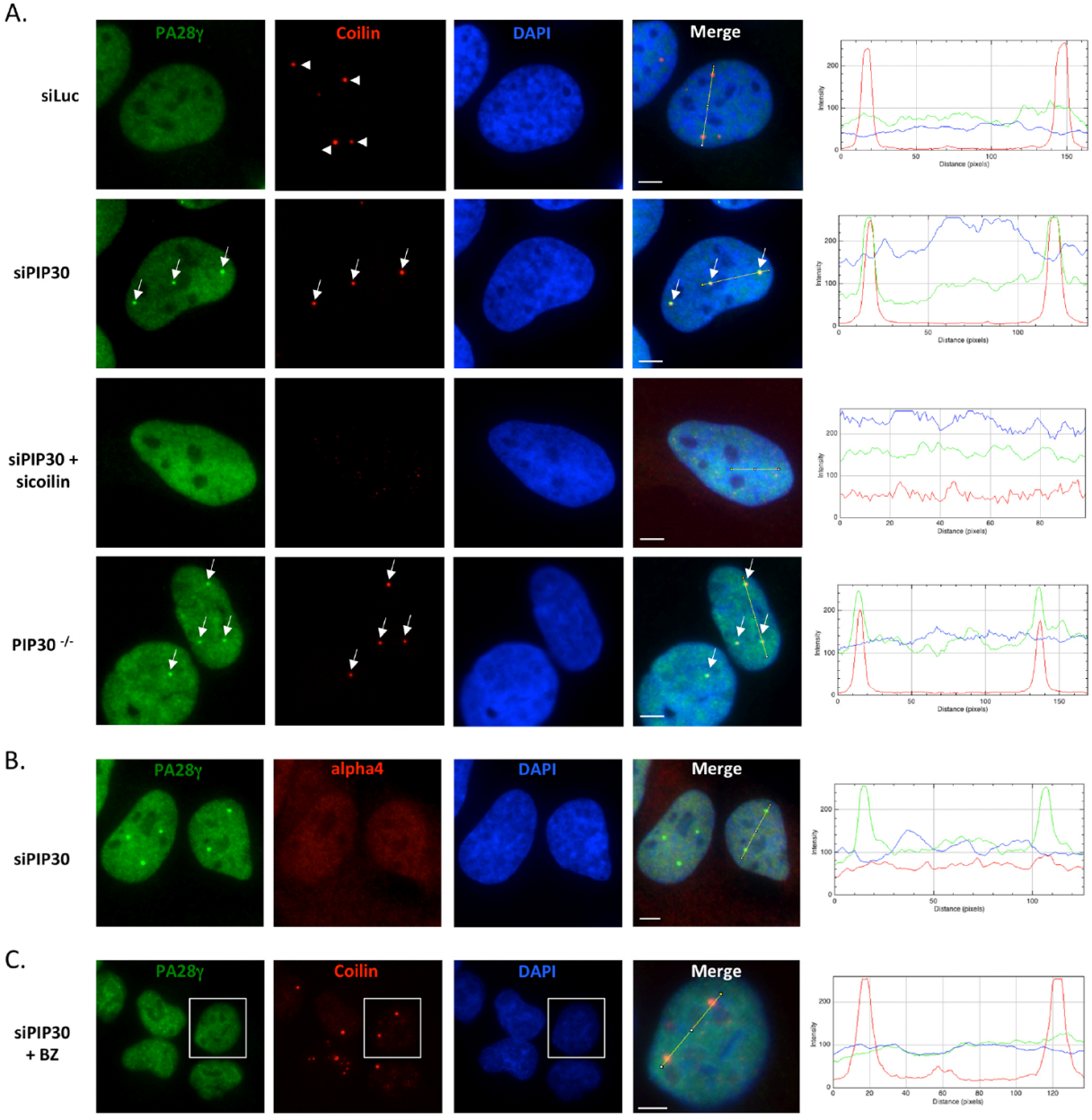

Fig. 7: PIP30 depletion induces the accumulation of PA28γ, but not the 20S core proteasome, in Cajal bodies

A. ***PIP30 depletion induces the accumulation of PA28γ in Cajal bodies.*** The co-localization of endogenous PA28γ and coilin was analyzed by indirect immunofluorescence in U2OS cells treated either with a control siRNA (siLuc), a siRNA targeting PIP30 or siRNAs targeting both PIP30 and coilin, and in PIP30 $^{-/-}$ cells. The coilin signal is indicated in red, the PA28γ signal in green and the DAPI signal in blue. **Right panels**: Profile plots, generated using ImageJ, display in two-dimensional graphs the pixel intensities of the green, the red and the blue signals, along the yellow lines drawn on the merge images. Bars, 10 µm.

B. ***The 20S proteasome does not accumulate in CBs together with PA28γ, after PIP30 depletion.*** The co-localization between PA28γ and the α4-subunit of the 20S core proteasome (the latter used as a signature for the presence of the whole 20S core complex) was analyzed by immunofluorescence in cells depleted for PIP30 by siRNAs. The α4 signal is in red, the PA28γ signal in green and the DAPI signal in blue. A profile plot, similar to those of Fig. 7A, is shown (right panel). Bars, 10 μm.

C. ***Proteasome inhibition prevents the accumulation of PA28γ in CBs.*** The co-localization between PA28γ and coilin was analyzed by indirect immunofluorescence in PIP30-depleted cells, treated with 10 nM bortezomib (BZ). The coilin signal is in red, the PA28γ signal in green and the DAPI signal in blue. A profile plot, similar to those of Fig. 7A, is shown (right panel). Bars, 10 μm.

543 cells, suggesting that PA28γ function in CBs could be proteasome independent in these
544 conditions.
545 Given that the PA28γ/coilin interaction is enhanced upon UV-C (Cioce et al., 2006), it
546 was tempting to speculate that the accumulation of PA28γ in CBs in PIP30 -/- cells is
547 linked to an increased association between PA28γ and coilin. We checked this
548 hypothesis, both by co-immunoprecipitation and PLA. Figure 8A shows a weak
549 interaction between coilin and PA28γ in control cells, which is strongly enhanced (> 5
550 fold) in PIP30 -/- cells. In agreement with this result, we observed that the number of
551 PLA dots per cell, which reports the interaction between PA28γ and coilin, was higher in
552 PIP30 -/- cells, as compared with control cells (101 versus 44) (Fig. 8B). We conclude
553 that the absence of PIP30 favors the association between PA28γ and coilin. Interestingly,
554 we could not detect any interaction between coilin and PIP30 by co-IP and by PLA (Fig.
555 2A, S4A and S4B). This suggests that the association between PA28γ and either PIP30 or
556 coilin is mutually exclusive and therefore strongly supports the idea that PIP30
557 modulates PA28γ function in CB dynamics by competing with coilin for PA28γ
558 interaction.
559
560 DISCUSSION
561
562 In this study we report the identification of a novel and specific interaction partner of
563 PA28γ, called FAM192A or NIP30 (NEFA Interacting Nuclear Protein 30 kDa) in
564 databanks (UniProtKB - Q9GZU8), by a high throughput approach combining SILAC-
565 based mass spectrometry and co-immunoprecipitation of endogenous PA28γ. The
566 function of this protein is currently unknown and the origin of the NIP30 name itself is

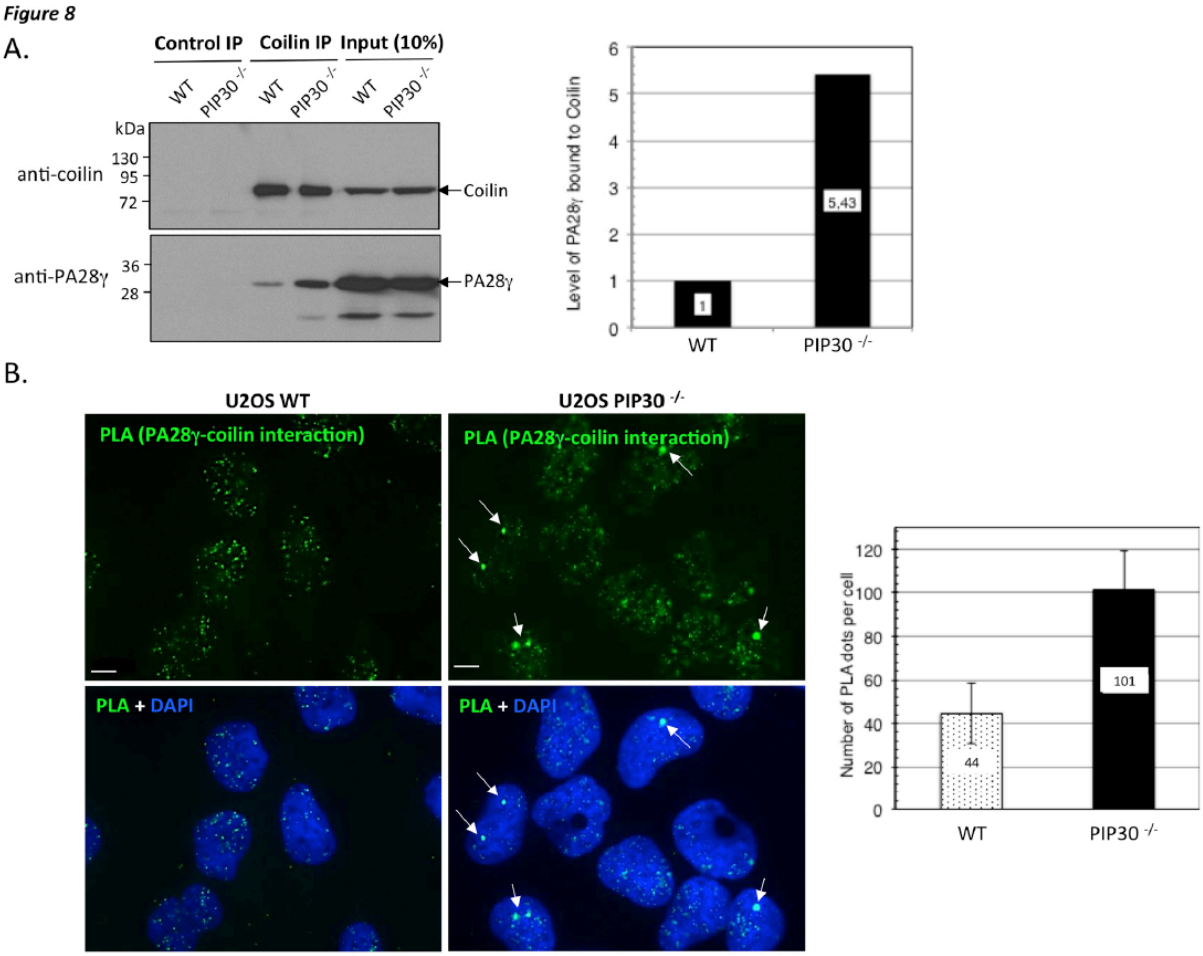

Fig. 8: PIP30 depletion increases the interaction of PA28γ with coilin

A. PIP30 depletion increases the co-immunoprecipitation of PA28γ with endogenous coilin. Cell extracts from asynchronously growing parental (WT) or PIP30 $^{-/-}$ U2OS cells were incubated with control IgG or anti-coilin antibodies. Immunocomplexes were analyzed by SDS-PAGE, probed for the indicated proteins (left panel), and the amount of PA28γ associated with coilin was quantified and normalized to the amount of immunoprecipitated coilin (right panel).

B. PIP30 depletion leads to an increased interaction between PA28γ and coilin by PLA. To examine endogenous interactions between PA28γ and coilin, asynchronously growing parental (WT) or PIP30 $^{-/-}$ U2OS cells were subjected to an *in situ* proximity ligation assay (PLA) using anti-PA28γ (mouse) and anti-coilin (rabbit) antibodies (left panel), and the number of PLA dots was quantified using the ImageJ software (right panel). Data represent the mean of two independent experiments (n= 123 WT cells and 112 PIP30 $^{-/-}$ cells). Bars, 10 µm.

not clear, although it has been postulated that the term "NEFA" could refer to "Non Esterified Fatty Acids". Interestingly, our SILAC IPs reciprocally identified both PA28γ and FAM192A as the most abundant interaction partner of the other. Several large-scale proteomic studies have also identified FAM192A together with PA28γ in the same complexes (Barth et al., 2014; Huttlin et al., 2015; Tsuruta et al., 2016; Wan et al., 2015). Therefore, we propose to rename FAM192A to "PA28γ Interacting Protein 30kDa" (PIP30), to highlight the physical and functional links between these two proteins.

We show here that PA28γ interacts with the C-terminal domain of PIP30 and that CK2-dependent phosphorylation of a conserved acidic and serine-rich sequence located in this PIP30 C-terminal region plays a crucial role in the stabilization of the PIP30/PA28γ complex. Of note, mutation of the putative phosphorylated serine residues (S222 and S228) reduced interaction with PA28γ, albeit not preventing binding completely. We hypothesize that multiple serine residues can be phosphorylated in this region, due to the multisite phosphorylation activity of CK2 (St-Denis et al., 2015). Consistent with this, the Global Proteome Machine (GPM) data repository indicates that serines S219, S221, S222 and S224 on PIP30 (Accession: ENSP00000335808) are phosphorylated *in vivo* (Craig et al., 2004). We propose therefore that the cluster of negative charges carried both by the acidic and the phosphorylated serine residues in the PIP30 C-terminus is critical for increasing the overall stability of the PIP30-PA28γ complex and could possibly constitute an anchorage site for positively charged residues in PA28γ.

Given that CK2-dependent phosphorylation of PIP30 is important for its interaction with PA28γ, it is tempting to postulate that the regulation of CK2 activity may affect the formation of the PIP30/PA28γ complex. However, CK2 is a ubiquitous and pleiotropic kinase, involved in the phosphorylation of more than 20% of the whole proteome (Salvi

et al., 2009). Furthermore, CK2 inhibition during 24 h reduces but does not completely abolish PIP30 phosphorylation levels *in cellulo*. This result, together with the fact that PA28γ-bound PIP30 cannot be dephosphorylated by λ-phosphatase, suggests a slow turnover of the phosphate groups for the fraction of endogenous PIP30 complexed with PA28γ (more than 50%). For example, phosphorylated serines located at the interface between PIP30 and PA28γ may be inaccessible to phosphatases as long as the complex is stable. Altogether, these observations suggest that physiological destabilization of the PIP30/PA28γ interaction might involve structural changes in the PIP30/PA28γ complex that weaken the interface between the two proteins, thereby controlling the accessibility of PIP30 phosphorylation sites to phosphatases.

By investigating whether PIP30 could affect the function of PA28γ in the regulation of CB dynamics (Cioce et al., 2006), we observed that non-synchronized PIP30 -/- and PA28γ -/- cells have opposite phenotypes regarding CB integrity, suggesting that PIP30 and PA28γ have antagonistic roles in this process. Interestingly, PIP30 depletion led to a strong decrease in the number of CBs and to an increased interaction between coilin and PA28γ, similarly to PA28γ overexpression and UV-C treatment (Cioce et al., 2006). However, a key feature of PIP30 depletion was the presence of residual CBs, in which PA28γ accumulated, whereas PA28γ overexpression and UV-C treatment induced an almost complete loss of CBs (Cioce et al., 2006). Of note, to our knowledge, PA28γ has only been observed to accumulate in CBs once before, in a study by Lafarga and colleagues in SMA motor neurons (Tapia et al., 2012). In these pathologic neurons, the assembly of CBs is impaired, due to the lack of SMN, an essential CB component (Lefebvre et al., 1995; Lemm et al., 2006; Liu and Dreyfuss, 1996). These neurons nevertheless possess residual CB structures that contain PA28γ (Tapia et al., 2012),

similarly to what we observed here in PIP30 -/- cells. It has been shown that CBs are kinetic structures (Carmo-Fonseca et al., 1993) and therefore the phenotype observed in both PIP30 $^{-/-}$ cells and SMA motor neurons, i.e., the accumulation of PA28γ in residual CBs, could reflect the fact that these residual CBs are stalled at intermediate stages of assembly/disassembly, in line with our hypothesis that PA28γ stimulates CB disruption and/or inhibits CB formation. Alternatively, the absence of PIP30 may result in the formation of defective CB structures that are not normally present in wild type cells.

This raises an intriguing question: what are the mechanisms underlying PA28γ-mediated CB disruption in either PIP30 $^{-/-}$, or in PA28γ-overexpressing cells? One obvious possibility is that PA28γ could target CB components for degradation by the proteasome, since it is known that CBs are disrupted in cells lacking CB components, such as SMN, PHAX and WRAP53 (Lemm et al., 2006; Mahmoudi et al., 2010), and that the proteasome-dependent degradation of FLASH upon UV-C results in the disappearance of CB-associated Histone Locus bodies (Barcaroli et al., 2006; Bongiorno-Borbone et al., 2010). However, we could not detect 20S proteasome α4 subunit accumulation in CBs, together with PA28γ, upon PIP30 depletion. In addition, we could not detect any interaction between 20S proteasome α6 subunit and GFP-coilin, either in wild-type, or in PIP30 -/- cells. Finally, proteasome inhibition, which stimulates the recruitment of PA28γ to the 20S proteasome, prevented the accumulation of PA28γ in CBs in PIP30 -/- cells. Taken together, these findings suggest that the function of PA28γ in CB dynamics could be proteasome-independent. Interestingly, the increase in CB number observed in bortezomib-treated cells by Lafarga and colleagues (Palanca et al., 2014) is in agreement with our data and could be explained by the fact that proteasome

655 inhibition favors the formation of PA28γ/20S proteasome complexes to the detriment of
656 PA28γ/coilin complexes.
657 Importantly, CB disruption strongly correlates with an increase in the formation of the
658 PA28γ/coilin complex in 1) UV-C-treated cells, 2) PIP30-depleted cells and 3) PA28γ-
659 overexpressing cells. Therefore, another possibility to explain PA28γ-mediated CB
660 disruption could be that the PA28γ/coilin complex interferes with coilin functioning as a
661 CB scaffold protein, for example by inhibiting the association of coilin either with itself,
662 or with other CB components, such as Sm proteins, SMN, etc., or both. In this context, our
663 results suggest a model in which PIP30 competes with coilin for its interaction with
664 PA28γ. When PIP30 is absent, the association between PA28γ and coilin is favored,
665 leading to a decrease in the number of CBs. Similarly, GFP-PA28γ overexpression
666 presumably increases the pool of free PA28γ, i.e., not bound to PIP30, and therefore
667 leads to both an increased interaction of PA28γ with coilin, as seen in our GFP-PA28γ
668 SILAC pull-down, and consequent CB disruption (Cioce et al., 2006). In agreement with
669 this hypothesis, we could not detect PIP30 and coilin in the same complex, either by
670 GFP-PIP30 SILAC IP, or by GFP-coilin IP. We thus propose that the abundance of the
671 PA28γ/coilin complex is a critical parameter for CB stability and that PIP30 could
672 buffer/sequester PA28γ away from coilin, in a phosphorylation-dependent manner,
673 thereby providing a reversible mechanism for regulating CB formation through the
674 opposing action of kinases/phosphatases that modulate the interaction between PIP30
675 and PA28γ. However, given that we observed an important overall stability of the
676 PIP30/PA28γ complex, it is possible that the interaction between PIP30 and PA28γ
677 might be only locally regulated, possibly in the vicinity of CBs.

678 The role of PIP30 and PA28γ in CB dynamics might be especially important during the
679 cellular stress response. In particular, PA28γ has been shown to participate in CB
680 disruption upon UV-C treatment (Cioce et al., 2006). Therefore, an attractive hypothesis
681 is that PIP30/PA28γ interaction could be down-regulated upon UV-C treatment.
682 However, we could not detect a significant and reproducible change in the levels of
683 PIP30/PA28γ association that could alone explain both the increased interaction of
684 PA28γ with coilin and CB fragmentation in UV-C-treated cells. As discussed above, a
685 possible explanation is that PIP30/PA28γ interaction is regulated locally and that the
686 change in the overall population of PIP30/PA28γ complexes is too subtle to be detected.
687 However, additional mechanisms, more complex than the simple dissociation of the
688 PIP30/PA28γ complex, may also be at play during UV-C-induced CB disruption.
689 Interestingly, like PA28γ, coilin is recruited to DNA damage sites upon genotoxic stress
690 (Bártová et al., 2014; Suchánková et al., 2015). Given that the association between PA28γ
691 and coilin mostly occurs outside CBs and that this interaction is increased upon DNA
692 damage, such as UV-C treatment, one can imagine that these two proteins might act in
693 concert in the DNA damage response and exert a common function that is not limited to
694 CB disruption. Therefore, it will be interesting to analyze the relationship between
695 PA28γ and coilin under different types of stresses and investigate the function of PIP30
696 in these processes.
697 Altogether, our results in this study provide important insights into the function of the
698 previously uncharacterized FAM192A/PIP30 protein and indicate that PIP30 plays an
699 important role in regulating the proteasome activator PA28γ, linking it to the control of
700 Cajal body dynamics, nuclear organization and participation in cellular stress responses.
701

MATERIALS AND METHODS

Antibodies and other reagents

The sources of the antibodies used in this study were as follows: anti-PA28γ (rabbit polyclonal, BML-PW8190, ENZO Life Sciences; rabbit polyclonal, 383900, Zymed/Life Technologies; rabbit polyclonal, PD003, MBL; mouse monoclonal, 611180, BD Transduction), anti-GFP (rabbit polyclonal, TP401, Torrey Pines Biolabs), anti-coilin (mouse monoclonal 5P10 (Rebelo et al., 1996) for indirect immunofluorescence, rabbit polyclonal PLA 0290, Sigma-Aldrich, for PLA and IPs, rabbit polyclonal R288 (Andrade et al., 1993) for WB), anti-β–actin (rabbit monoclonal, 13E5, Cell Signalling), anti-α-tubulin (mouse monoclonal, T9026, Sigma-Aldrich). The anti-FAM192A/PIP30 rabbit polyclonal antibody was raised against full-length protein (UniProtKB - Q9GZU8) and affinity-purified (home-made). Fluorescent secondary antibodies conjugated either to AlexaFluor 488, 594 and 633, or to DyLight 680 and 800, were purchased from Molecular Probes and ThermoFisher Scientific, respectively. Secondary antibodies conjugated to HRP were purchased from BioRad.

Recombinant Casein Kinase 2 was purchased from New England Biolabs (P6010S) and CK2 inhibitor CX-4945 from Selleckchem (S2248).

Plasmids, subcloning and mutagenesis

pEGFP-C1 FAM192A/PIP30 was generated by inserting FAM192A cDNA (GenBank NP_079222.1, IMAGE 6305656) into pEGFP-C1 plasmid (Clontech), using HindIII and BamH1 restriction sites. FAM192A/PIP30 truncation and point mutation variants were then obtained either by PCR amplification or by site-directed mutagenesis.

For Cas9-mediated gene disruption, guide RNAs targeting PIP30 (GCCTCTTACCATGTTTTCTGAGG) and PSME3/PA28γ (GGAAGTGAAGCTCAAGGTAGCGG)

were selected using ChopChop (https://chopchop.rc.fas.harvard.edu/index.php) and corresponding oligonucleotides were subcloned in pMLM3636 (gift from Keith Joung, Addgene, plasmid # 43860) and pUC57-U6 (gift from Edouard Bertrand's laboratory). For PIP30 depletion, 800 bp PIP30 right and left DNA homology arms were obtained by gene synthesis (IDT, USA) and subcloned in HR110PA-1 vector (SBI, Palo Alto, USA).

RNA interference

Silencing RNAs targeting PA28γ and FAM192A/PIP30 were obtained from Dharmacon (On target plus Human PSME3 siRNA 5 nmol (J-012133-05-0005) and SMARTpool On target plus Human FAM192A (L-014528-01), respectively). Silencing RNA targeting coilin was obtained from IDT (AGAGTCGAGAGAACAATA).

Cell culture and transfection

U2OS (HTB-96) and HeLa (CCL-2) cell lines were obtained from ATCC. Cells were grown in DMEM (4.5 g/L glucose) (Lonza) supplemented with 10% heat inactivated FBS (Sigma-Aldrich), 2 mM L-glutamine (Lonza), 10 U/ml penicillin and 10 μg/ml streptomycine (Lonza) in humid atmosphere containing 5% CO_2 at 37°C. Media of cell lines with stable expression of GFP constructs were additionally supplied with G418 (300 μg/ml).

Cells were typically transfected with 20 nM siRNA and 0.5 μg/ml DNA, using Lipofectamine RNAiMAX (Thermo Fisher Scientific) and Jet-PEI (Ozyme) transfection reagents respectively, according to manufacturer's instructions. Cells were treated and analyzed two days after siRNA transfection and one day after DNA transfection.

U2OS PIP30 -/- cells were generated by co-transfection of PIP30 sgGuide, pJDS246-WT CAS9 (gift from Keith Joung, Addgene, plasmid # 43861) and PIP30 HR110PA-1 vector

752 using Turbofect (Thermofischer) (Fu et al., 2014). PSME3/PA28γ -/- cells were
753 generated by cotransfection of PSME3/PA28γ sgGuide and pX459 vectors. Both PIP30
754 and PSME3/PA28γ -/- cells were selected with puromycine (1 μg/ml). Single clones
755 were then expanded and analyzed by western blotting using PIP30 and PA28γ
756 antibodies.
757 To generate stable GFP-PA28γ and GFP-FAM192A/PIP30 U2OS cell lines, parental U2OS
758 cells were transfected with peGFP-C1 PA28γ and peGFP-C1 FAM192A/PIP30 plasmids
759 and positive clones were selected in G418-containing medium.
760
761 *Production and purification of recombinant PIP30 and GST-PIP30*
762 Recombinant PIP30 was produced in *E. coli* BL21 DE3 Codon Plus bacteria as a 6His-
763 tagged protein and efficiently purified by affinity purification followed by proteolytic
764 cleavage of the tag, ion exchange chromatography and gel filtration. Full-length protein
765 was then used for rabbit immunization. GST-fusion proteins were produced in bacteria
766 and efficiently purified using glutathione sepharose beads. In the kinase assay, purified
767 GST-fusion proteins were buffer exchanged in PBS kinase buffer.
768
769 *Pulldown and immunoprecipitation*
770 For immunoprecipitation of GFP-fusion proteins, U2OS cells were transfected with the
771 indicated constructs. Twenty-four hours post-transfection, cells were homogenized in
772 lysis buffer (25 mM HEPES pH 7.8, 100 mM KCl, 10 mM $MgCl_2$, 1 mM EDTA, 1% IGEPAL
773 CA-630, 0.1% Triton X-100, 1 mM DTT, 1 mM ATP, 10% glycerol (v/v)), in the presence
774 of complete EDTA free protease inhibitor cocktail (Roche), for 15 min on ice. After
775 centrifugation at 15000 g for 15 min (4°C), supernatants were recovered and protein
776 concentration was determined by Bradford assays. 20 μl of GFP-TRAP-A® beads

(Chromotek) were used per IP, mixed with 200 μg of protein extract and incubated with constant gentle stirring for 1 h at 4°C. Beads were washed three times with lysis buffer and boiled in 2X Laemmli sample buffer. Samples were then analyzed by SDS-PAGE and immunoblotting.

Endogenous PIP30 and PA28γ were immunoprecipitated from 150 μg (Fig. 5C) or 500 μg (Fig. 2D and S2B) of total cell extracts using anti-PIP30 (rabbit) and anti-PA28γ (rabbit) antibodies, bound to protein A magnetic beads (Dynal, Lake Success, NY) for 2 h at 4°C.

For co-immunoprecipitation of coilin and PA28γ proteins (Fig. 8A), nuclear extracts were prepared as described in (Cioce et al., 2006). Briefly, U2OS and PIP30 -/- cell pellets were resuspended in hypotonic buffer (10 mM Tris-HCl pH 7.5, 10% glycerol, 4 mM DTT, 50 mM NaF, 1 mM Na_3VO_4, 1 mM $MgCl_2$) in the presence of complete EDTA-free protease inhibitor cocktail (Roche). IGEPAL CA-630 was then added at the final concentration of 0.5% and cells were incubated on ice for 3 min. After centrifugation at 800 g for 5 min, the nuclei, present in the pellet, were resuspended in digestion buffer (2 mM Tris-HCl pH 8.5, 20% glycerol, 10 mM DTT, 50 mM NaF, 1 mM Na_3VO_4, 1 mM $MgCl_2$, 5 mM $CaCl_2$, 1X complete protease inhibitor cocktail) supplemented with 75 U/ml micrococcal nuclease, and then digested for 15 min at 25°C with constant stirring. At the end, an equivalent volume of extraction buffer (2 mM Tris-HCl pH 8.5, 50 mM NaF, 1 mM Na_3VO_4, 1 mM $MgCl_2$, 20 mM EDTA, 0.84 M KCl, 1X complete protease inhibitor cocktail) was added and the mix was incubated on ice for 20 min. Nuclear extracts were clarified by centrifugation for 30 min at 15000 g. Before immunoprecipitation, KCl concentration was reduced to 280 mM, 3 μg of anti-coilin or control IgG were added to 400 μg of nuclear extracts and incubated for 2 h at 4°C. Immunoprecipitated proteins were collected by addition of 15 μl of protein A-sepharose beads. After extensive washes,

beads were boiled in 2X Laemmli sample buffer and samples were analyzed by SDS-PAGE and immunoblotting.

For GST pull-down, phosphorylated GST-PIP30 proteins were incubated with recombinant PA28γ in 50 mM Tris-HCl pH 7.5, 50 mM NaCl, 5 mM EDTA for 15 min then diluted in PBS and purified on glutathione sepharose beads. Beads were washed 3 times in PBS and proteins eluted by boiling in sample buffer.

Cell fixation, immunofluorescence microscopy and PLA assays

Cells were fixed in 3.7% paraformaldehyde/PBS for 10 min at room temperature (RT), washed with PBS and permeabilized in PBS containing 1% Triton X-100 for 15 min at RT. Coverslips were then blocked in blocking solution (1% FBS, 0.01% Tween-20/PBS) for 10-20 min and incubated with primary antibodies, diluted in blocking buffer, for 1 h at RT or 37°C in a humidified atmosphere. After three washes in PBS, coverslips were incubated with Alexa-Fluor conjugated secondary antibodies, diluted in blocking solution for 40 min at RT. Coverslips were washed with PBS, incubated with 0.1 μg/ml DAPI solution in PBS for 5 min at RT, washed twice in PBS and finally once in H_2O. Coverslips were mounted on glass slides using ProLong Gold antifade reagent (Thermo Fisher Scientific).

For proximity ligation assays (PLA), cells on coverslips were fixed in 3.7% paraformaldehyde/PBS for 20 min at RT, washed three times in PBS and permeabilized twice, first in PBS containing 0.25% Triton X-100 for 5 min at RT, washed three times in PBS and second in 100% cold methanol for 10 min at -20°C. After a step of rehydration by three washes in PBS (3 x 3 min at RT), coverslips were incubated in the blocking solution provided by the Duolink® kit. Cells were then incubated with anti-PA28γ (mouse) and anti-PIP30 (rabbit) antibodies as described above. Duolink® *In Situ* PLA

827 Probe Anti-Rabbit MINUS and Anti-Mouse PLUS and Duolink® *In Situ* Detection
828 Reagents (Sigma-Aldrich) were used, according to the manufacturer's instructions.
829
830 *Image acquisition and analysis*
831 Z-stacks and images were acquired with a 63 X/1.4 NA or 40 X/1.3 NA oil immersion
832 objective lenses using widefield microscopes, DM6000 (Leica Microsystems) or
833 Axioimager Z1 or Z2 (Carl Zeiss), equipped with coolSNAP HQ2 cameras (Photometrics).
834 Images were acquired as TIF files using MetaMorph imaging software (Molecular
835 Devices). Profile plots were generated in ImageJ software. For CB quantitative analysis,
836 CBs were stained with mouse monoclonal anti-coilin primary antibody (5P10) and Goat
837 anti-Rabbit IgG (H+L) secondary antibody, Alexa Fluor® 488. Z-stacks were acquired
838 every 0.4 µm (Z step) with a range of 10 µm to image the whole nuclei. Specific band
839 pass filters were used, BPem 340-380 and BPex 450-490 to detect DAPI and BPem 450-
840 490 BPex 500-550 to detect AlexaFluor 488. The size, the intensity and the number of
841 Cajal bodies were detected with ImageJ (1.49v). A specific "macro" has been created to
842 automatically quantify these different parameters. The script allows to create a mask of
843 DAPI image to isolate the nucleus of each cell and create a maximum intensity projection
844 (MIP) of the 25 Z-stacks. The mask is used in the MIP to count the number of Cajal
845 bodies of each nucleus via an appropriate thresholding. The "Analyze Particles" tool of
846 ImageJ was used to calculate the size and the mean gray value of each Cajal body.
847 The statistical analysis was done using the R software. For both graphs "% of CB positive
848 cells" and "% of cells with 3 CBs and more", a chi-squared statistic test and a pairwise
849 comparison of proportions were used. For both graphs "Mean area of CBs" and Mean
850 intensity of CBs", a one-way ANOVA test and t-tests with non-pooled SD were used. P-
851 values < 0,001 were indicated by 3 asterisks ***.

In vitro CK2 phosphorylation assay

GST and GST-PIP30-H201 proteins were incubated with recombinant CK2 according to the manufacturer's instructions. For radioactive kinase assays, ^{33}P labeled ATP (1 μCi/100 μM) was included. Reactions were stopped either by adding 5 mM EDTA or Laemmli sample buffer.

SILAC IPs and mass spectrometry analysis

SILAC IPs (endogenous PA28γ, GFP-PA28γ and GFP-FAM192A/PIP30) were essentially performed as previously described in (Boulon et al., 2010). Briefly, parental U2OS and stable GFP-PA28γ and GFP-PIP30 U2OS cells were grown in DMEM medium for SILAC (ThermoFisher, 89985) supplemented with 10% dialyzed FCS and penicillin/streptomycin for 10 days. L-arginine (R0) (84 mg/ml, Sigma-Aldrich) and L-lysine (K0) (146 mg/ml, Sigma-Aldrich) were added to the light (L) medium, L-$^{13}C_6$-arginine (R6) and L-4,4,5,5-D_4-lysine (K4) (Cambridge Isotope Laboratories) were added to the medium (M) medium and L-$^{13}C_6$,$^{15}N_4$-arginine (R10) and L-$^{13}C_6$,$^{15}N_4$-lysine (K8) (or L-$^{13}C_6$- arginine (R6) and L-$^{13}C_6$-lysine (K6)) (Cambridge Isotope Laboratories) were added to the heavy (H) medium. Ten 140-mm diameter culture dishes were used per SILAC condition. When indicated, cells were treated with MG132 proteasome inhibitor (25 μM) for 7 h. Whole cell extracts were prepared by lysing cells in 1X RIPA buffer (50 mM Tris-HCl pH 7.5, 150 mM NaCl, 1% IGEPAL CA-630, 0.5% DOC, protease inhibitor cocktail), sonicating 3 x 10 s on ice and centrifugating at 2800 g for 10 min at 4°C to remove cell debris. For nuclear extracts, cells were incubated in buffer A (20 mM Tris-HCl pH 7.4, 10 mM KCl, 3 mM $MgCl_2$, 0.1% IGEPAL CA-630, 10% glycerol, protease

878 inhibitor cocktail) for 10 min at 4°C, with occasional mixing. Nuclei were then
879 centrifugated at 1430 g for 10 min at 4°C, resuspended in S1 solution (0.25 M sucrose,
880 10 mM $MgCl_2$, protease inhibitor cocktail) and layered over a cushion of S3 solution
881 (0.88 M sucrose, 0.5 mM $MgCl_2$, protease inhibitor cocktail). After centrifugation at 2800
882 g for 10 min at 4°C, a cleaner nuclear pellet was obtained, which was resuspended in 1X
883 RIPA buffer (50 mM Tris-HCl pH 7.5, 150 mM NaCl, 1% IGEPAL CA-630, 0.5% DOC,
884 protease inhibitor cocktail), sonicated 5 x 10 s on ice, to ensure release of as many
885 nuclear proteins as possible, and centrifuged at 2800 g for 10 min at 4°C to pellet debris.
886 Prior to endogenous PA28γ IP, control rabbit IgG and anti-PA28γ antibodies (rabbit
887 polyclonal ZYMED and MBL) were covalently coupled to protein G-dynabeads (Thermo
888 Fisher Scientific). Nuclear extracts were precleared by incubation with protein G-
889 dynabeads alone and separate IPs were then performed in parallel by incubating the
890 same amount of proteins from L and M extracts on control and anti-PA28γ-beads,
891 respectively. For GFP-PA28γ and GFP-PIP30 IPs, extracts were precleared with protein
892 G-sepharose beads alone and separate IPs were then performed by incubating the same
893 amount of proteins from L, M and H extracts with GFP-TRAP_A affinity matrix
894 (Chromotek) for 1 h at 4°C. After several washes, bound proteins were eluted in 1% SDS,
895 boiled for 10 min, reduced and alkylated and then separated by SDS-PAGE. After tryptic
896 *in gel* digestion, peptides were analyzed by LC-MS/MS (LTQ-Orbitrap XL, Thermo Fisher
897 Scientific Inc.). Data were then analyzed and quantified by MaxQuant (version 1.0.12.31)
898 (Cox et al., 2009) and the Mascot search engine (Matrix Science, version 2.2.2) software,
899 as in (Boulon et al., 2010).
900
901 ACKNOWLEDGMENTS

We thank Drs Douglas Lamont and Kenneth Beattie of the Fingerprints Proteomics Facility at the University of Dundee for technical assistance with the MS analysis. We thank the Montpellier Ressources Imagerie (MRI) facility, member of the France-BioImaging infrastructure, for providing state of the art equipment and expertise in image analysis and software development. We address our special thanks to Cédric Hassen Khodja for the statistical analyses. We thank the CRBM animal house for the production of rabbit polyclonal antibodies. We are grateful to the past and current members of the Coux and Lamond laboratories for their advice and suggestions.

The authors declare no competing financial interests.

AUTHOR CONTRIBUTIONS

S.B. and O.C. conceived the project. SILAC IPs were performed by S.B and Douglas Lamont (Dundee Fingerprints Proteomics Facility). Recombinant PIP30 was purified by B.J.N. and O.C. Rabbit anti-PIP30 antibody was purified and characterized by B.J.N, F.M. and C.B.A. Endogenous PIP30 and PA28γ IPs were performed by C.B.A. PLA experiments were performed by V.B. B.J.N., D.F. and F.M. performed the molecular biology work. GST- and GFP-PIP30 pull-down experiments were performed by B.J.N and D.F. Phosphorylation studies and the production of the gene-edited cell lines were performed by D.F. and V.B. S.B. analyzed CB dynamics in PA28γ -/- and PIP30 -/- cells. V.B. and D.F. analyzed the localization of PA28γ in PIP30 -/- cells. Coilin IPs were performed by V.B. The original draft was written by S.B. All authors discussed the results and commented on the manuscript.

NON STANDARD ABBREVIATIONS

926 CB : Cajal body ; CK2 : Casein Kinase 2 ; H/L ratio : Heavy/Light ratio ; IP :
927 Immunoprecipitation ; PIP30 : PA28γ Interacting Protein 30kDa ; PLA : Proximity
928 Ligation Assay ; SILAC : Stable Isotope Labeling by Amino-Acids in Cell Culture ; U2OS :
929 human OsteoSarcoma cell line.
930
931
932
933 REFERENCES
934
935 Andrade, L.E., Tan, E.M., Chan, E.K., 1993. Immunocytochemical analysis of the coiled
936 body in the cell cycle and during cell proliferation. Proc. Natl. Acad. Sci. U. S. A. 90,
937 1947–1951.
938 Baldin, V., Militello, M., Thomas, Y., Doucet, C., Fic, W., Boireau, S., Jariel-Encontre, I.,
939 Piechaczyk, M., Bertrand, E., Tazi, J., Coux, O., 2008. A novel role for PA28gamma-
940 proteasome in nuclear speckle organization and SR protein trafficking. Mol. Biol.
941 Cell 19, 1706–1716. doi:10.1091/mbc.E07-07-0637
942 Barcaroli, D., Dinsdale, D., Neale, M.H., Bongiorno-Borbone, L., Ranalli, M., Munarriz, E.,
943 Sayan, A.E., McWilliam, J.M., Smith, T.M., Fava, E., Knight, R.A., Melino, G., De
944 Laurenzi, V., 2006. FLASH is an essential component of Cajal bodies. Proc. Natl.
945 Acad. Sci. U. S. A. 103, 14802–14807. doi:10.1073/pnas.0604225103
946 Barth, T.K., Schade, G.O.M., Schmidt, A., Vetter, I., Wirth, M., Heun, P., Thomae, A.W.,
947 Imhof, A., 2014. Identification of novel Drosophila centromere-associated
948 proteins. Proteomics 14, 2167–2178. doi:10.1002/pmic.201400052
949 Bártová, E., Foltánková, V., Legartová, S., Sehnalová, P., Sorokin, D.V., Suchánková, J.,
950 Kozubek, S., 2014. Coilin is rapidly recruited to UVA-induced DNA lesions and γ-

radiation affects localized movement of Cajal bodies. Nucl. Austin Tex 5, 460–468. doi:10.4161/nucl.29229

Bongiorno-Borbone, L., De Cola, A., Barcaroli, D., Knight, R.A., Di Ilio, C., Melino, G., De Laurenzi, V., 2010. FLASH degradation in response to UV-C results in histone locus bodies disruption and cell-cycle arrest. Oncogene 29, 802–810. doi:10.1038/onc.2009.388

Boulon, S., Ahmad, Y., Trinkle-Mulcahy, L., Verheggen, C., Cobley, A., Gregor, P., Bertrand, E., Whitehorn, M., Lamond, A.I., 2010. Establishment of a protein frequency library and its application in the reliable identification of specific protein interaction partners. Mol. Cell. Proteomics MCP 9, 861–879. doi:10.1074/mcp.M900517-MCP200

Carmo-Fonseca, M., Ferreira, J., Lamond, A.I., 1993. Assembly of snRNP-containing coiled bodies is regulated in interphase and mitosis--evidence that the coiled body is a kinetic nuclear structure. J. Cell Biol. 120, 841–852.

Cesaro, L., Pinna, L.A., 2015. The generation of phosphoserine stretches in phosphoproteins: mechanism and significance. Mol. Biosyst. 11, 2666–2679. doi:10.1039/c5mb00337g

Chai, F., Liang, Y., Bi, J., Chen, L., Zhang, F., Cui, Y., Bian, X., Jiang, J., 2014. High expression of REGγ is associated with metastasis and poor prognosis of patients with breast cancer. Int. J. Clin. Exp. Pathol. 7, 7834–7843.

Chen, D., Yang, X., Huang, L., Chi, P., 2013. The expression and clinical significance of PA28 γ in colorectal cancer. J. Investig. Med. Off. Publ. Am. Fed. Clin. Res. 61, 1192–1196. doi:10.2310/JIM.0000000000000001

Chen, X., Barton, L.F., Chi, Y., Clurman, B.E., Roberts, J.M., 2007. Ubiquitin-independent degradation of cell-cycle inhibitors by the REGgamma proteasome. Mol. Cell 26,

843–852. doi:10.1016/j.molcel.2007.05.022

Cioce, M., Boulon, S., Matera, A.G., Lamond, A.I., 2006. UV-induced fragmentation of Cajal bodies. J. Cell Biol. 175, 401–413. doi:10.1083/jcb.200604099

Cioce, M., Lamond, A.I., 2005. Cajal bodies: a long history of discovery. Annu. Rev. Cell Dev. Biol. 21, 105–131. doi:10.1146/annurev.cellbio.20.010403.103738

Cox, J., Matic, I., Hilger, M., Nagaraj, N., Selbach, M., Olsen, J.V., Mann, M., 2009. A practical guide to the MaxQuant computational platform for SILAC-based quantitative proteomics. Nat. Protoc. 4, 698–705. doi:10.1038/nprot.2009.36

Craig, R., Cortens, J.P., Beavis, R.C., 2004. Open source system for analyzing, validating, and storing protein identification data. J. Proteome Res. 3, 1234–1242. doi:10.1021/pr049882h

Dong, S., Jia, C., Zhang, S., Fan, G., Li, Y., Shan, P., Sun, L., Xiao, W., Li, L., Zheng, Y., Liu, J., Wei, H., Hu, C., Zhang, W., Chin, Y.E., Zhai, Q., Li, Q., Liu, J., Jia, F., Mo, Q., Edwards, D.P., Huang, S., Chan, L., O'Malley, B.W., Li, X., Wang, C., 2013. The REGγ proteasome regulates hepatic lipid metabolism through inhibition of autophagy. Cell Metab. 18, 380–391. doi:10.1016/j.cmet.2013.08.012

Dundr, M., Ospina, J.K., Sung, M.-H., John, S., Upender, M., Ried, T., Hager, G.L., Matera, A.G., 2007. Actin-dependent intranuclear repositioning of an active gene locus in vivo. J. Cell Biol. 179, 1095–1103. doi:10.1083/jcb.200710058

Fu, Y., Reyon, D., Joung, J.K., 2014. Targeted genome editing in human cells using CRISPR/Cas nucleases and truncated guide RNAs. Methods Enzymol. 546, 21–45. doi:10.1016/B978-0-12-801185-0.00002-7

Gao, X., Li, J., Pratt, G., Wilk, S., Rechsteiner, M., 2004. Purification procedures determine the proteasome activation properties of REG gamma (PA28 gamma). Arch. Biochem. Biophys. 425, 158–164. doi:10.1016/j.abb.2004.03.021

1001 Girard, C., Neel, H., Bertrand, E., Bordonné, R., 2006. Depletion of SMN by RNA
1002 interference in HeLa cells induces defects in Cajal body formation. Nucleic Acids
1003 Res. 34, 2925–2932. doi:10.1093/nar/gkl374
1004 He, J., Cui, L., Zeng, Y., Wang, G., Zhou, P., Yang, Y., Ji, L., Zhao, Y., Chen, J., Wang, Z., Shi, T.,
1005 Zhang, P., Chen, R., Li, X., 2012. REGγ is associated with multiple oncogenic
1006 pathways in human cancers. BMC Cancer 12, 75. doi:10.1186/1471-2407-12-75
1007 Hebert, M.D., 2013. Signals controlling Cajal body assembly and function. Int. J. Biochem.
1008 Cell Biol. 45, 1314–1317. doi:10.1016/j.biocel.2013.03.019
1009 Huttlin, E.L., Ting, L., Bruckner, R.J., Gebreab, F., Gygi, M.P., Szpyt, J., Tam, S., Zarraga, G.,
1010 Colby, G., Baltier, K., Dong, R., Guarani, V., Vaites, L.P., Ordureau, A., Rad, R.,
1011 Erickson, B.K., Wühr, M., Chick, J., Zhai, B., Kolippakkam, D., Mintseris, J., Obar,
1012 R.A., Harris, T., Artavanis-Tsakonas, S., Sowa, M.E., De Camilli, P., Paulo, J.A.,
1013 Harper, J.W., Gygi, S.P., 2015. The BioPlex Network: A Systematic Exploration of
1014 the Human Interactome. Cell 162, 425–440. doi:10.1016/j.cell.2015.06.043
1015 Kaiser, T.E., Intine, R.V., Dundr, M., 2008. De novo formation of a subnuclear body.
1016 Science 322, 1713–1717. doi:10.1126/science.1165216
1017 Kish-Trier, E., Hill, C.P., 2013. Structural biology of the proteasome. Annu. Rev. Biophys.
1018 42, 29–49. doi:10.1146/annurev-biophys-083012-130417
1019 Kobayashi, T., Wang, J., Al-Ahmadie, H., Abate-Shen, C., 2013. ARF regulates the stability
1020 of p16 protein via REGγ-dependent proteasome degradation. Mol. Cancer Res.
1021 MCR 11, 828–833. doi:10.1158/1541-7786.MCR-13-0207
1022 Lefebvre, S., Bürglen, L., Reboullet, S., Clermont, O., Burlet, P., Viollet, L., Benichou, B.,
1023 Cruaud, C., Millasseau, P., Zeviani, M., 1995. Identification and characterization of
1024 a spinal muscular atrophy-determining gene. Cell 80, 155–165.
1025 Lemm, I., Girard, C., Kuhn, A.N., Watkins, N.J., Schneider, M., Bordonné, R., Lührmann, R.,

2006. Ongoing U snRNP biogenesis is required for the integrity of Cajal bodies. Mol. Biol. Cell 17, 3221–3231. doi:10.1091/mbc.E06-03-0247

Levy-Barda, A., Lerenthal, Y., Davis, A.J., Chung, Y.M., Essers, J., Shao, Z., van Vliet, N., Chen, D.J., Hu, M.C.-T., Kanaar, R., Ziv, Y., Shiloh, Y., 2011. Involvement of the nuclear proteasome activator PA28γ in the cellular response to DNA double-strand breaks. Cell Cycle Georget. Tex 10, 4300–4310. doi:10.4161/cc.10.24.18642

Li, J., Feng, X., Sun, C., Zeng, X., Xie, L., Xu, H., Li, T., Wang, R., Xu, X., Zhou, X., Zhou, M., Zhou, Y., Dan, H., Wang, Z., Ji, N., Deng, P., Liao, G., Geng, N., Wang, Y., Zhang, D., Lin, Y., Ye, L., Liang, X., Li, L., Luo, G., Jiang, L., Wang, Z., Chen, Q., 2015. Associations between proteasomal activator PA28γ and outcome of oral squamous cell carcinoma: Evidence from cohort studies and functional analyses. EBioMedicine 2, 851–858. doi:10.1016/j.ebiom.2015.07.004

Li, L., Dang, Y., Zhang, J., Yan, W., Zhai, W., Chen, H., Li, K., Tong, L., Gao, X., Amjad, A., Ji, L., Jing, T., Jiang, Z., Shi, K., Yao, L., Song, D., Liu, T., Yang, X., Yang, C., Cai, X., Xu, W., Huang, Q., He, J., Liu, J., Chen, T., Moses, R.E., Fu, J., Xiao, J., Li, X., 2015. REGγ is critical for skin carcinogenesis by modulating the Wnt/β-catenin pathway. Nat. Commun. 6, 6875. doi:10.1038/ncomms7875

Li, L., Zhao, D., Wei, H., Yao, L., Dang, Y., Amjad, A., Xu, J., Liu, J., Guo, L., Li, D., Li, Z., Zuo, D., Zhang, Y., Liu, J., Huang, S., Jia, C., Wang, L., Wang, Y., Xie, Y., Luo, J., Zhang, B., Luo, H., Donehower, L.A., Moses, R.E., Xiao, J., O'Malley, B.W., Li, X., 2013. REGγ deficiency promotes premature aging via the casein kinase 1 pathway. Proc. Natl. Acad. Sci. U. S. A. 110, 11005–11010. doi:10.1073/pnas.1308497110

Li, L.-P., Cheng, W.-B., Li, H., Li, W., Yang, H., Wen, D.-H., Tang, Y.-D., 2012. Expression of proteasome activator REGγ in human laryngeal carcinoma and associations with

1051 tumor suppressor proteins. Asian Pac. J. Cancer Prev. APJCP 13, 2699–2703.
1052 Li, S., Jiang, C., Pan, J., Wang, X., Jin, J., Zhao, L., Pan, W., Liao, G., Cai, X., Li, X., Xiao, J., Jiang,
1053 J., Wang, P., 2015. Regulation of c-Myc protein stability by proteasome activator
1054 REGγ. Cell Death Differ. 22, 1000–1011. doi:10.1038/cdd.2014.188
1055 Li, X., Amazit, L., Long, W., Lonard, D.M., Monaco, J.J., O'Malley, B.W., 2007. Ubiquitin- and
1056 ATP-independent proteolytic turnover of p21 by the REGgamma-proteasome
1057 pathway. Mol. Cell 26, 831–842. doi:10.1016/j.molcel.2007.05.028
1058 Li, X., Lonard, D.M., Jung, S.Y., Malovannaya, A., Feng, Q., Qin, J., Tsai, S.Y., Tsai, M.-J.,
1059 O'Malley, B.W., 2006. The SRC-3/AIB1 coactivator is degraded in a ubiquitin- and
1060 ATP-independent manner by the REGgamma proteasome. Cell 124, 381–392.
1061 doi:10.1016/j.cell.2005.11.037
1062 Liu, Q., Dreyfuss, G., 1996. A novel nuclear structure containing the survival of motor
1063 neurons protein. EMBO J. 15, 3555–3565.
1064 Machyna, M., Neugebauer, K.M., Staněk, D., 2015. Coilin: The first 25 years. RNA Biol. 12,
1065 590–596. doi:10.1080/15476286.2015.1034923
1066 Mahmoudi, S., Henriksson, S., Weibrecht, I., Smith, S., Söderberg, O., Strömblad, S.,
1067 Wiman, K.G., Farnebo, M., 2010. WRAP53 is essential for Cajal body formation
1068 and for targeting the survival of motor neuron complex to Cajal bodies. PLoS Biol.
1069 8, e1000521. doi:10.1371/journal.pbio.1000521
1070 Mao, I., Liu, J., Li, X., Luo, H., 2008. REGgamma, a proteasome activator and beyond? Cell.
1071 Mol. Life Sci. CMLS 65, 3971–3980. doi:10.1007/s00018-008-8291-z
1072 Matera, A.G., Wang, Z., 2014. A day in the life of the spliceosome. Nat. Rev. Mol. Cell Biol.
1073 15, 108–121. doi:10.1038/nrm3742
1074 Meggio, F., Pinna, L.A., 2003. One-thousand-and-one substrates of protein kinase CK2?
1075 FASEB J. Off. Publ. Fed. Am. Soc. Exp. Biol. 17, 349–368. doi:10.1096/fj.02-

0473rev

Moncsek, A., Gruner, M., Meyer, H., Lehmann, A., Kloetzel, P.-M., Stohwasser, R., 2015. Evidence for anti-apoptotic roles of proteasome activator 28γ via inhibiting caspase activity. Apoptosis Int. J. Program. Cell Death 20, 1211–1228. doi:10.1007/s10495-015-1149-6

Moriishi, K., Mochizuki, R., Moriya, K., Miyamoto, H., Mori, Y., Abe, T., Murata, S., Tanaka, K., Miyamura, T., Suzuki, T., Koike, K., Matsuura, Y., 2007. Critical role of PA28gamma in hepatitis C virus-associated steatogenesis and hepatocarcinogenesis. Proc. Natl. Acad. Sci. U. S. A. 104, 1661–1666. doi:10.1073/pnas.0607312104

Moriishi, K., Okabayashi, T., Nakai, K., Moriya, K., Koike, K., Murata, S., Chiba, T., Tanaka, K., Suzuki, R., Suzuki, T., Miyamura, T., Matsuura, Y., 2003. Proteasome activator PA28gamma-dependent nuclear retention and degradation of hepatitis C virus core protein. J. Virol. 77, 10237–10249.

Morris, G.E., 2008. The Cajal body. Biochim. Biophys. Acta 1783, 2108–2115. doi:10.1016/j.bbamcr.2008.07.016

Murata, S., Kawahara, H., Tohma, S., Yamamoto, K., Kasahara, M., Nabeshima, Y., Tanaka, K., Chiba, T., 1999. Growth retardation in mice lacking the proteasome activator PA28gamma. J. Biol. Chem. 274, 38211–38215.

Nie, J., Wu, M., Wang, J., Xing, G., He, F., Zhang, L., 2010. REGgamma proteasome mediates degradation of the ubiquitin ligase Smurf1. FEBS Lett. 584, 3021–3027. doi:10.1016/j.febslet.2010.05.034

Nizami, Z., Deryusheva, S., Gall, J.G., 2010. The Cajal body and histone locus body. Cold Spring Harb. Perspect. Biol. 2, a000653. doi:10.1101/cshperspect.a000653

Novotný, I., Blažíková, M., Staněk, D., Herman, P., Malinsky, J., 2011. In vivo kinetics of

1101 U4/U6·U5 tri-snRNP formation in Cajal bodies. Mol. Biol. Cell 22, 513–523.
1102 doi:10.1091/mbc.E10-07-0560
1103 Novotný, I., Malinová, A., Stejskalová, E., Matějů, D., Klimešová, K., Roithová, A., Švéda, M.,
1104 Knejzlík, Z., Staněk, D., 2015. SART3-Dependent Accumulation of Incomplete
1105 Spliceosomal snRNPs in Cajal Bodies. Cell Rep. doi:10.1016/j.celrep.2014.12.030
1106 Okamura, T., Taniguchi, S.-I., Ohkura, T., Yoshida, A., Shimizu, H., Sakai, M., Maeta, H.,
1107 Fukui, H., Ueta, Y., Hisatome, I., Shigemasa, C., 2003. Abnormally high expression
1108 of proteasome activator-gamma in thyroid neoplasm. J. Clin. Endocrinol. Metab.
1109 88, 1374–1383. doi:10.1210/jc.2002-021413
1110 Palanca, A., Casafont, I., Berciano, M.T., Lafarga, M., 2014. Reactive nucleolar and Cajal
1111 body responses to proteasome inhibition in sensory ganglion neurons. Biochim.
1112 Biophys. Acta 1842, 848–859. doi:10.1016/j.bbadis.2013.11.016
1113 Pickering, A.M., Davies, K.J.A., 2012. Degradation of damaged proteins: the main function
1114 of the 20S proteasome. Prog. Mol. Biol. Transl. Sci. 109, 227–248.
1115 doi:10.1016/B978-0-12-397863-9.00006-7
1116 Pierre, F., Chua, P.C., O'Brien, S.E., Siddiqui-Jain, A., Bourbon, P., Haddach, M., Michaux, J.,
1117 Nagasawa, J., Schwaebe, M.K., Stefan, E., Vialettes, A., Whitten, J.P., Chen, T.K.,
1118 Darjania, L., Stansfield, R., Anderes, K., Bliesath, J., Drygin, D., Ho, C., Omori, M.,
1119 Proffitt, C., Streiner, N., Trent, K., Rice, W.G., Ryckman, D.M., 2011. Discovery and
1120 SAR of 5-(3-chlorophenylamino)benzo[c][2,6]naphthyridine-8-carboxylic acid
1121 (CX-4945), the first clinical stage inhibitor of protein kinase CK2 for the
1122 treatment of cancer. J. Med. Chem. 54, 635–654. doi:10.1021/jm101251q
1123 Poh, Y.-C., Shevtsov, S.P., Chowdhury, F., Wu, D.C., Na, S., Dundr, M., Wang, N., 2012.
1124 Dynamic force-induced direct dissociation of protein complexes in a nuclear body
1125 in living cells. Nat. Commun. 3, 866. doi:10.1038/ncomms1873

1126 Rebelo, L., Almeida, F., Ramos, C., Bohmann, K., Lamond, A.I., Carmo-Fonseca, M., 1996.
1127 The dynamics of coiled bodies in the nucleus of adenovirus-infected cells. Mol.
1128 Biol. Cell 7, 1137–1151.
1129 Roessler, M., Rollinger, W., Mantovani-Endl, L., Hagmann, M.-L., Palme, S., Berndt, P.,
1130 Engel, A.M., Pfeffer, M., Karl, J., Bodenmüller, H., Rüschoff, J., Henkel, T., Rohr, G.,
1131 Rossol, S., Rösch, W., Langen, H., Zolg, W., Tacke, M., 2006. Identification of PSME3
1132 as a novel serum tumor marker for colorectal cancer by combining two-
1133 dimensional polyacrylamide gel electrophoresis with a strictly mass
1134 spectrometry-based approach for data analysis. Mol. Cell. Proteomics MCP 5,
1135 2092–2101. doi:10.1074/mcp.M600118-MCP200
1136 Salvi, M., Sarno, S., Cesaro, L., Nakamura, H., Pinna, L.A., 2009. Extraordinary pleiotropy
1137 of protein kinase CK2 revealed by weblogo phosphoproteome analysis. Biochim.
1138 Biophys. Acta 1793, 847–859. doi:10.1016/j.bbamcr.2009.01.013
1139 Shibatani, T., Carlson, E.J., Larabee, F., McCormack, A.L., Früh, K., Skach, W.R., 2006.
1140 Global organization and function of mammalian cytosolic proteasome pools:
1141 Implications for PA28 and 19S regulatory complexes. Mol. Biol. Cell 17, 4962–
1142 4971. doi:10.1091/mbc.E06-04-0311
1143 St-Denis, N., Gabriel, M., Turowec, J.P., Gloor, G.B., Li, S.S.-C., Gingras, A.-C., Litchfield,
1144 D.W., 2015. Systematic investigation of hierarchical phosphorylation by protein
1145 kinase CK2. J. Proteomics 118, 49–62. doi:10.1016/j.jprot.2014.10.020
1146 Strzelecka, M., Trowitzsch, S., Weber, G., Lührmann, R., Oates, A.C., Neugebauer, K.M.,
1147 2010. Coilin-dependent snRNP assembly is essential for zebrafish
1148 embryogenesis. Nat. Struct. Mol. Biol. 17, 403–409. doi:10.1038/nsmb.1783
1149 Suchánková, J., Kozubek, S., Legartová, S., Sehnalová, P., Küntziger, T., Bártová, E., 2015.
1150 Distinct kinetics of DNA repair protein accumulation at DNA lesions and cell

cycle-dependent formation of γH2AX- and NBS1-positive repair foci. Biol. Cell 107, 440–454. doi:10.1111/boc.201500050

Sun, L., Fan, G., Shan, P., Qiu, X., Dong, S., Liao, L., Yu, C., Wang, T., Gu, X., Li, Q., Song, X., Cao, L., Li, X., Cui, Y., Zhang, S., Wang, C., 2016. Regulation of energy homeostasis by the ubiquitin-independent REGγ proteasome. Nat. Commun. 7, 12497. doi:10.1038/ncomms12497

Tapia, O., Bengoechea, R., Palanca, A., Arteaga, R., Val-Bernal, J.F., Tizzano, E.F., Berciano, M.T., Lafarga, M., 2012. Reorganization of Cajal bodies and nucleolar targeting of coilin in motor neurons of type I spinal muscular atrophy. Histochem. Cell Biol. 137, 657–667. doi:10.1007/s00418-012-0921-8

Tomko, R.J., Hochstrasser, M., 2013. Molecular architecture and assembly of the eukaryotic proteasome. Annu. Rev. Biochem. 82, 415–445. doi:10.1146/annurev-biochem-060410-150257

Trinkle-Mulcahy, L., Sleeman, J.E., 2016. The Cajal body and the nucleolus: "In a relationship" or "It's complicated"? RNA Biol. 1–13. doi:10.1080/15476286.2016.1236169

Tsuruta, F., Takebe, A., Haratake, K., Kanemori, Y., Kim, J., Endo, T., Kigoshi, Y., Fukuda, T., Miyahara, H., Ebina, M., Baba, T., Chiba, T., 2016. SCFFbl12 Increases p21Waf1/Cip1 Expression Level through Atypical Ubiquitin Chain Synthesis. Mol. Cell. Biol. 36, 2182–2194. doi:10.1128/MCB.00174-16

Waddell, D.S., Duffin, P.J., Haddock, A.N., Triplett, V.E., Saredy, J.J., Kakareka, K.M., Eldredge, J.T., 2016. Isolation, expression analysis and characterization of NEFA-interacting nuclear protein 30 and RING finger and SPRY domain containing 1 in skeletal muscle. Gene 576, 319–332. doi:10.1016/j.gene.2015.10.046

Wan, C., Borgeson, B., Phanse, S., Tu, F., Drew, K., Clark, G., Xiong, X., Kagan, O., Kwan, J.,

1176 Bezginov, A., Chessman, K., Pal, S., Cromar, G., Papoulas, O., Ni, Z., Boutz, D.R.,
1177 Stoilova, S., Havugimana, P.C., Guo, X., Malty, R.H., Sarov, M., Greenblatt, J., Babu,
1178 M., Derry, W.B., Tillier, E.R., Wallingford, J.B., Parkinson, J., Marcotte, E.M., Emili,
1179 A., 2015. Panorama of ancient metazoan macromolecular complexes. Nature 525,
1180 339–344. doi:10.1038/nature14877
1181 Wang, Q., Sawyer, I.A., Sung, M.-H., Sturgill, D., Shevtsov, S.P., Pegoraro, G., Hakim, O.,
1182 Baek, S., Hager, G.L., Dundr, M., 2016. Cajal bodies are linked to genome
1183 conformation. Nat. Commun. 7, 10966. doi:10.1038/ncomms10966
1184 Welk, V., Coux, O., Kleene, V., Abeza, C., Trümbach, D., Eickelberg, O., Meiners, S., 2016.
1185 Inhibition of Proteasome Activity Induces Formation of Alternative Proteasome
1186 Complexes. J. Biol. Chem. 291, 13147–13159. doi:10.1074/jbc.M116.717652
1187 Xiong, S., Zheng, Y., Jiang, P., Liu, R., Liu, X., Qian, J., Gu, J., Chang, L., Ge, D., Chu, Y., 2014.
1188 PA28gamma emerges as a novel functional target of tumour suppressor
1189 microRNA-7 in non-small-cell lung cancer. Br. J. Cancer 110, 353–362.
1190 doi:10.1038/bjc.2013.728
1191 Ying, H., Furuya, F., Zhao, L., Araki, O., West, B.L., Hanover, J.A., Willingham, M.C., Cheng,
1192 S.-Y., 2006. Aberrant accumulation of PTTG1 induced by a mutated thyroid
1193 hormone beta receptor inhibits mitotic progression. J. Clin. Invest. 116, 2972–
1194 2984. doi:10.1172/JCI28598
1195 Zannini, L., Buscemi, G., Fontanella, E., Lisanti, S., Delia, D., 2009.
1196 REGgamma/PA28gamma proteasome activator interacts with PML and Chk2 and
1197 affects PML nuclear bodies number. Cell Cycle Georget. Tex 8, 2399–2407.
1198 doi:10.4161/cc.8.15.9084
1199 Zannini, L., Lecis, D., Buscemi, G., Carlessi, L., Gasparini, P., Fontanella, E., Lisanti, S.,
1200 Barton, L., Delia, D., 2008. REGgamma proteasome activator is involved in the

maintenance of chromosomal stability. Cell Cycle Georget. Tex 7, 504–512.

Zhang, Y., Liu, S., Zuo, Q., Wu, L., Ji, L., Zhai, W., Xiao, J., Chen, J., Li, X., 2015. Oxidative challenge enhances REGγ-proteasome-dependent protein degradation. Free Radic. Biol. Med. 82, 42–49. doi:10.1016/j.freeradbiomed.2015.01.024

Table S1

Gene Names	Protein IDs	Protein Names	Unique Peptides	Sequence Coverage [%]	Ratio H/L	Intensity H
PSMA1	P25786	Proteasome subunit alpha type-1	14	52,4	39,747	7888600
PSME3	P61289	Proteasome activator complex subunit 3	25	76,8	14,914	2009700000
CEP152	O94986	Centrosomal protein of 152 kDa	3	2,5	12,05	3400400
SMARCA4	P51532	SMARCA4 isoform 2 (SWI/SNF related, matrix associated, actin dependen	16	20,1	6,2142	469900
BRD9	Q9H8M2	Bromodomain-containing protein 9	8	17,8	4,394	338740
NDUFS8	O00217	NADH dehydrogenase [ubiquinone] iron-sulfur protein 8, mitochondrial	7	36,2	3,982	33060000
MATR3	P43243	Matrin-3	2	5,1	3,7907	176150
FAM192A	Q9GZU8	NEFA-interacting nuclear protein NIP30	14	48	3,258	3433900
FAU	P62861	Ubiquitin-like protein FUBI;40S ribosomal protein S30	3	14,3	2,9776	86965
HNRNPL;HNRPL	P14866	Heterogeneous nuclear ribonucleoprotein L	4	7,1	2,675	775540
PLEC1	Q15149	Plectin-1;Hemidesmosomal protein 1;Plectin-11	3	68,4	2,5439	105370000
U2AF2;U2AF65	P26368	Splicing factor U2AF 65 kDa subunit	16	35,2	2,4359	5525600
U2AF1;U2AF35	Q01081	Splicing factor U2AF 35 kDa subunit	8	35	2,3661	5108200
HNRNPM;HNRPM	P52272	Heterogeneous nuclear ribonucleoprotein M	6	9,7	2,3499	2570200
SF3B3	Q15393	Splicing factor 3B subunit 3	8	8,3	2,3467	2011200
HNRNPF;HNRPF	P52597	Heterogeneous nuclear ribonucleoprotein F	2	13,5	2,3449	5383200
SF3B14	Q9Y3B4	Pre-mRNA branch site protein p14;SF3B 14 kDa subunit	5	47,2	2,1821	183820
BCLAF1	Q9NYF8	Bcl-2-associated transcription factor 1	6	6,1	2,1019	4912900
RPS26	P62854	40S ribosomal protein S26	4	37,4	2,0653	591760
RPL22	P35268	60S ribosomal protein L22	5	55,5	1,995	588410
SF3B1;SAP155	O75533	Splicing factor 3B subunit 1	20	19,1	1,992	11332000
RP9	Q8TA86	Retinitis pigmentosa 9 protein	14	49,3	1,9651	16962000
RBM39	Q14498	RNA-binding protein 39	22	52,1	1,9309	46370000
ERH	P84090	Enhancer of rudimentary homolog	6	51	1,7589	5241600
DHX9;DDX9	Q08211	ATP-dependent RNA helicase A;DEAH box protein 9	2	2,2	1,758	191250
SFRS12IP1	Q8N9Q2	Protein SFRS12IP1;p18SRP	4	21,4	1,726	1334100
MMTAG2	Q9BU76	Multiple myeloma tumor-associated protein 2	6	22,8	1,7134	597760
RPS27	P42677	40S ribosomal protein S27	2	39,3	1,7133	368970
ZCCHC17	Q9NP64	Nucleolar protein of 40 kDa	4	21	1,7021	587080
DHX15	O43143	DEAH box protein 15	4	5,8	1,6943	725370
SNRPD2;SNRPD1	P62316;A8K797	Small nuclear ribonucleoprotein Sm D2	7	55,1	1,5949	312580
DYNLL1	P63167	Dynein light chain 1, cytoplasmic	2	20,2	1,589	320610
DDX5	P17844	Probable ATP-dependent RNA helicase DDX5	13	30	1,5841	20552000
THRAP3;TRAP150	Q9Y2W1	Thyroid hormone receptor-associated protein 3	13	14,9	1,5195	13683000
PRPF40A	O75400	Pre-mRNA-processing factor 40 homolog A	5	25	1,4285	265810

Table S1: ***List of the PA28γ interaction partners identified in endogenous PA28γ SILAC IP (untreated cells).*** Only proteins identified with a significant H/L SILAC ratio (H/L ratio > 1.4) and containing at least two unique peptides identified are listed in this table. Proteins are classified by descending order for the H/L ratio.

Table S2

Gene Names	Protein IDs	Protein Names	Unique Peptides	Sequence Coverage [%]	Ratio H/L	Intensity H
PSMB6	P28072	Proteasome subunit beta type-6	5	19,7	61,825	9767900
PSMB5	P28074	Proteasome subunit beta type-5	9	36,9	52,022	22181000
EEF1G;EF1G	P26641	Elongation factor 1-gamma	2	4,5	29,713	851540
PSMA5	P28066	Proteasome subunit alpha type-5	11	60,6	26,761	32061000
PSMB3	P49720	Proteasome subunit beta type-3	8	45,9	26,549	28571000
PSMA3	P25788	Proteasome subunit alpha type-3	13	40,8	24,739	37334000
PLEC1	Q15149	Plectin-1	3	68,4	19,738	2023100000
PSMB2	P49721	Proteasome subunit beta type-2	11	64,7	15,326	20648000
NDUFS8	O00217	NADH dehydrogenase [ubiquinone] iron-sulfur protein 8, mitochondrial	6	36,2	15,058	6896600
TTN	Q8WZ42	Titin	2	0,1	14,016	191830
PSMD12	O00232	26S proteasome non-ATPase regulatory subunit 12	6	13,2	12,646	1334300
AP2S1;AP17	P53680	AP-2 complex subunit sigma-1coat assembly protein AP17	2	13,4	10,682	442660
PSME3	P61289	Proteasome activator complex subunit 3	21	76,8	10,552	670710000
PSMA2	P25787	Proteasome subunit alpha type-2	8	51,7	9,8303	22739000
VIM	P08670	Vimentin	35	83,7	9,6953	315740000
PSMA4	P25789	Proteasome subunit alpha type-4	10	47,5	9,6604	31401000
PSMA1	P25786	Proteasome subunit alpha type-1type	14	52,4	9,5647	22654000
PSMD7	P51665	26S proteasome non-ATPase regulatory subunit 7	7	30,2	9,3949	3070300
SMARCA4	P51532	SMARCA4 isoform 2 (SWI/SNF related, matrix associated, actin dependen	16	20,1	8,6871	31323000
BRE	Q9NXR7	Protein BRE	2	5,8	8,5646	326400
PSMB1	P20618	Proteasome subunit beta type-1	12	57,3	8,5341	41981000
KRT18	P05783	Keratin, type I cytoskeletal 18	16	66,7	8,4512	45191000
PSMD2	Q13200	26S proteasome non-ATPase regulatory subunit 22	14	22,5	8,1266	9468800
PSMB7	Q99436	Proteasome subunit beta type-7	9	43,3	8,0026	10857000
FAM192A; NIP30	Q9GZU8	NEFA-interacting nuclear protein NIP30	14	48	7,9182	17204000
RPS27A	P62979	40S ribosomal protein S27a;Ubiquitin	2	59,6	7,7174	153390000
HSPB1	P04792	Heat shock protein beta-1	9	59,5	7,716	9644100
CAV1	Q03135	Caveolin-1	6	41	7,2766	5718100
PSMD14	O00487	26S proteasome non-ATPase regulatory subunit 14	3	9,7	6,5297	1434000
PSMA6	P60900	Proteasome subunit alpha type-6	13	56,1	6,1175	47883000
PSMC5	P62195	26S protease regulatory subunit 8	13	41,1	6,1121	4765000
PSMD11	O00231	26S proteasome non-ATPase regulatory subunit 11	16	41,6	6,0466	4502500
PSMB4	P28070	Proteasome subunit beta type-4	8	47	5,9875	13090000
MYL6	P60660	Myosin light polypeptide 6	10	66,2	5,8686	6197400
MYH9	P35579	Myosin-9	74	69,5	5,7347	69254000
KRT8	P05787	Keratin, type II cytoskeletal 8	22	57,6	5,2887	28652000
RUVBL2	Q9Y230	RuvB-like 2	2	3,9	5,2244	125970
BAG2	O95816	BAG family molecular chaperone regulator 2	4	18	5,2078	754860
HSPA1A	P0DMV8	Heat shock 70 kDa protein 1	2	50,9	5,2065	38135000
PSMD8	P48556	26S proteasome non-ATPase regulatory subunit 8	3	9,1	5,0877	412950
KRT75	O95678	Keratin, type II cytoskeletal 75	3	22	4,8303	870110
PSMA7	O14818	Proteasome subunit alpha type-7	13	63,3	4,6955	66492000
PSMC6	P62333	26S protease regulatory subunit 10b	10	25,1	4,6081	4927600
PSMC2	P35998	26S protease regulatory subunit 7	9	22,2	4,399	1275300
KRT80	Q6KB66	Keratin, type II cytoskeletal 80	5	15,9	4,3462	172030
PSMD1	Q99460	26S proteasome non-ATPase regulatory subunit 1	16	23,5	4,299	4071000
KRT81	Q14533	Keratin type II cuticular Hb1	5	17	3,9881	1496600
MYO1C	O00159	MYO1C variant protein	18	22,4	3,9351	4249400
DHRS2	Q13268	Dehydrogenase/reductase SDR family member 2	14	52,5	3,8848	59972000
PLEC1	Q15149	Plectin-1	3	66,6	3,8655	720170
EIF2S1;EIF2A	P05198	Eukaryotic translation initiation factor 2 subunit 1	2	6,7	3,6806	159500
FLNC	Q14315	Filamin-C	70	36,7	3,6623	27721000
DBN1	Q16643	Drebrin	3	31,7	3,6587	594780
PSMC3	P17980	26S protease regulatory subunit 6A	6	17,8	3,5678	2305000
TUBA1B	P68363	Tubulin alpha-1B chain	9	34,8	3,5627	6845900
TUBG1	P23258	Tubulin gamma-1 chain	2	5,3	3,4215	52089
MYLC2B;MRLC2	O14950	Myosin regulatory light chain MRCL3 variant	7	60,5	3,3971	2176600
PSMB8	P28062	Proteasome subunit beta type-8	7	25	3,3699	1727800
HSPA8	P11142	Heat shock cognate 71 kDa protein	18	40,7	3,3545	16824000
PATZ1	Q9HBE1	POZ-, AT hook-, and zinc finger-containing protein 1	3	5,2	3,3295	370370
HSPA6	P17066	Heat shock 70 kDa protein 6	2	17	3,3082	278710
PSMC1	P62191	26S protease regulatory subunit 4	10	30,7	3,2831	6846300
TRIM3	O75382	Tripartite motif-containing protein 3	8	14,4	3,1483	1357700
PSMC4	P43686	26S protease regulatory subunit 6b	14	42,3	3,1386	4133100
PSMD6	Q15008	26S proteasome non-ATPase regulatory subunit 6	9	27,8	2,9424	2199000
SLC25A5	P05141	ADP/ATP translocase 2	4	46,3	2,9396	7577900
CDC2	P06493	Cell division control protein 2 homolog	3	12,9	2,8838	381250
PSMD3	O43242	26S proteasome non-ATPase regulatory subunit 3	6	12,9	2,845	1072400
C14orf145	Q6ZU80	Uncharacterized protein C14orf145	26	26	2,775	6507100
BCLAF1	Q9NYF8	Bcl-2-associated transcription factor 1	2	6,1	2,7631	461620
ACTN1	P12814	ACTN1 protein;Alpha-actinin-1	24	33,3	2,7362	2734900
VCP	P55072	Transitional endoplasmic reticulum ATPase	2	3,7	2,718	94480
TUBB	P07437	Tubulin beta chain	10	31,3	2,712	4185400
RPS16	P62249	RPS16 protein	3	18,4	2,6838	265480
HNRNPC;HNRPC	P07910	Heterogeneous nuclear ribonucleoproteins C1/C2	9	26,5	2,623	4029500
PRKDC	P78527	DNA-dependent protein kinase catalytic subunit	17	5	2,5587	1728900
MAGED1	Q9Y5V3	Melanoma-associated antigen D1;MAGE-D1 antigen	3	4,1	2,555	544220
RPL10	P27635	Ribosomal protein L10	6	24,3	2,5515	2168700
RPS11	P62280	40S ribosomal protein S11	11	62	2,5078	7270100
HNRNPL;HNRPL	P14866	Heterogeneous nuclear ribonucleoprotein L	2	7,1	2,4448	180740
AHNAK	Q09666	Neuroblast differentiation-associated protein AHNAK	3	3,3	2,4253	474050
PGAM5	Q96HS1	Phosphoglycerate mutase family member 5;Bcl-XL-binding protein v68	3	8,7	2,4212	279720
SMARCA2	P51531	Probable global transcription activator SNF2L2	4	13,2	2,4183	321390
ERH	P84090	Enhancer of rudimentary homolog	5	51	2,4071	6174500
ARMS	Q9ULH0	Ankyrin repeat-rich membrane spanning protein	15	8,8	2,3827	2478000
ODF2	Q5BJF6	Outer dense fiber protein 2	12	17,1	2,3489	949610
THRAP3;TRAP150	Q9Y2W1	Thyroid hormone receptor-associated protein 3	7	14,9	2,2423	965170
PSMD13	Q9UNM6	26S proteasome non-ATPase regulatory subunit 13	9	26,7	2,2115	1592700
SNRPB	P14678	Small nuclear ribonucleoprotein-associated proteins B and B'	5	13,5	2,2042	1432000
CEP192	Q8TEP8	Centrosomal protein of 192 kDa	7	3,9	2,1847	206740

CEP192	Q8TEP8	Centrosomal protein of 192 kDa	7	3,9	2,1847	206740
CPSF3;CPSF73	Q9UKF6	Cleavage and polyadenylation specificity factor subunit 3	3	3,9	2,172	155710
NONO	Q15233	Non-POU domain-containing octamer-binding protein	2	3,4	2,1383	164970
SNRPE	P62304	Small nuclear ribonucleoprotein E	3	38	2,127	1158800
RPS8	P62241	40S ribosomal protein S8	2	9,2	2,1227	284950
CRYAB	P02511	Alpha-crystallin B chain	5	28	2,1176	602830
CPSF2	Q9P2I0	Cleavage and polyadenylation specificity factor subunit 2specificity factor	7	10,1	2,1149	1885400
SNRPD1	P62314	Small nuclear ribonucleoprotein Sm D1	4	29,5	2,1125	3027200
NES	P48681	Nestin	7	5,4	2,1061	521030
RPS6	P62753	40S ribosomal protein S6	2	8	2,1005	1326500
PHB	P35232	Prohibitin	2	11	2,0867	222650
RPL23	P62829	60S ribosomal protein L23	6	49,3	2,0801	6558700
SNRPA	P09012	U1 small nuclear ribonucleoprotein A	3	13,1	2,0553	1120500
SNRPD3	P62318	Small nuclear ribonucleoprotein Sm D3	3	22,9	2,0303	3728700
DYNLL1	P63167	Dynein light chain 1, cytoplasmic	2	20,2	2,0247	165010
RPS27	P42677	40S ribosomal protein S27	2	39,3	2,0206	2477900
RPS15A	P62244	40S ribosomal protein S15a	5	35,4	2,0098	1582700
CPSF1;CPSF160	Q10570	Cleavage and polyadenylation specificity factor subunit 1	28	22,3	1,9554	12720000
MYH10	P35580	Myosin-10	11	17,2	1,936	1770700
SLC25A3	Q00325	Phosphate carrier protein, mitochondrial	2	5,2	1,9244	150070
RPL35A;GIG33	P18077	60S ribosomal protein L35a	2	19,1	1,9188	433950
RPL18A	Q02543	60S ribosomal protein L18a	3	17	1,9125	259600
SNRPD2	P62316	Small nuclear ribonucleoprotein Sm D2;snRNP core protein D2	7	55,1	1,909	3895800
TCOF1	Q13428	Treacle protein;Treacher Collins syndrome protein	5	4,2	1,9083	666670
PHB2	Q99623	Prohibitin-2	2	7,7	1,9024	22974
RPL19	P84098	60S ribosomal protein L19	4	20,9	1,8814	1009700
PRDX1	Q06830	Peroxiredoxin-1	3	15,6	1,8731	756900
CAPZA1	P52907	F-actin-capping protein subunit alpha-1	2	11,5	1,8715	136010
EEF1A1	P68104	Elongation factor 1-alpha 1	4	11,9	1,7968	1857800
SON	P18583	SON protein	5	2,6	1,7954	1134400
RPLP0	P05388	60S acidic ribosomal protein P0	4	19,9	1,7799	397940
H2AFZ;H2AZ	P0C0S5	Histone H2A.Z	2	31,2	1,7758	24681000
FLNA	P21333	Filamin-A	17	11,6	1,7751	3018500
RPS9	P46781	40S ribosomal protein S9	9	40,2	1,7605	1770400
SFRS10;TRA2B	P62995	Splicing factor, arginine/serine-rich 10 (Transformer 2 homolog, Drosophi	2	8	1,7589	348010
RPL12	P30050	60S ribosomal protein L12	4	40	1,748	259850
RPS14	P62263	40S ribosomal protein S14	3	22,5	1,7157	2671300
DHX15	O43143	Putative pre-mRNA-splicing factor ATP-dependent RNA helicase DHX15	4	5,8	1,6883	804320
HNRNPU	Q00839	Heterogeneous nuclear ribonucleoprotein U (Scaffold attachment factor A	9	15,2	1,6782	4381200
HNRNPF;HNRPF	P52597	Heterogeneous nuclear ribonucleoprotein F	2	13,5	1,6759	3242300
HIST1H1C;H1F2	P16403	Histone H1.2	3	18,3	1,6654	706140
PRPF8;PRPC8	Q6P2Q9	Pre-mRNA-processing-splicing factor 8	7	2,7	1,6585	1172900
HIST1H4A;H4/A;H4FA;HIST1H	P62805	Histone H4	8	59,2	1,6565	20986000
EFTUD2	Q15029	116 kDa U5 small nuclear ribonucleoprotein component	6	7,6	1,6418	1291000
FBL	P22087	rRNA 2'-O-methyltransferase fibrillarin	5	17,1	1,5973	755820
TAF8	Q7Z7C8	Transcription initiation factor TFIID subunit 8	4	17	1,583	400000
HNRNPM;HNRPM	P52272	Heterogeneous nuclear ribonucleoprotein M	3	9,7	1,5652	691950
DDX5	P17844	Probable ATP-dependent RNA helicase DDX5	8	30	1,527	6114200
ASCC3L1;HELIC2	O75643	U5 small nuclear ribonucleoprotein 200 kDa helicase	25	14,7	1,52	5070900

Table S2: ***List of the PA28γ interaction partners identified in endogenous PA28γ SILAC IP (MG132-treated cells).*** Only proteins identified with a significant H/L SILAC ratio (H/L ratio > 1.5) and containing at least two unique peptides identified are listed in this table. Proteins are classified by descending order for the H/L ratio.

Table S3

Gene names	Protein IDs	Protein names	Unique peptides	Sequence coverage [%]	Ratio H/L	Intensity H
GFP	Q9U6Y5	Green Fluorescent Protein	11	53	44,917	15118000000
UBB;RPS27A;UBC;UBA52;UBE	J3QS39;J3QTR3;	Ubiquitin-60S ribosomal protein L40;Ubiquitin;60S ribosomal protein L40	4	50,5	26,981	265340000
PSME3	P61289	Proteasome activator complex subunit 3	28	86,2	16,491	36430000000
FAM192A;NIP30	Q9GZU8	Protein FAM192A	12	63,5	15,779	182930000
PSMA7;PSMA8	O14818;Q8TAA3	Proteasome subunit alpha type-7;Proteasome subunit alpha type-7-like	2	12,9	3,7274	3118600
COIL	P38432	Coilin	3	5,9	2,6545	3095400
VDAC2	P45880	Voltage-dependent anion-selective channel protein 2	3	16,5	1,6517	6038600
RCC2	Q9P258	Protein RCC2	2	5,2	1,5253	6408700
CAPZA1	P52907	F-actin-capping protein subunit alpha-1	6	46,2	1,4971	53597000
CAPZB	P47756	F-actin-capping protein subunit beta	4	17,3	1,4463	9878300
KPNB1	Q14974	Importin subunit beta-1	2	3,2	1,4106	2802800

Table S3: ***List of the PA28γ interaction partners identified in GFP-PA28γ SILAC IP.*** Only proteins identified with a significant H/L SILAC ratio (H/L ratio > 1.4) and containing at least two unique peptides identified are listed in this table. Proteins are classified by descending order for the H/L ratio.